AZƏRBAYCAN ALİ TEXNİKİ MƏKTƏBLƏRİNİN
XƏBƏRLƏRİ

NEWS
OF AZERBAIJAN HIGHER TECHNICAL EDUCATIONAL INSTITUTIONS

ИЗВЕСТИЯ
ВЫСШИХ ТЕХНИЧЕСКИХ УЧЕБНЫХ ЗАВЕДЕНИЙ АЗЕРБАЙДЖАНА

Cild 23. № 5
Vol. 23. № 5
Том 23. № 5

Azərbaycan Ali Texniki Məktəblərinin

X Ə B Ə R L Ə R İ

BAŞ REDAKTOR: PROFESSOR MUSTAFA BABANLI
Baş redaktor müavini – Rauf Əliyarov
Məsul katib – Oleq Hüseynov

REDAKSİYA HEYƏTİ:
V.M. Əhmədov, İ.A. Qaraqaş, H.B. Quliyev, R.S. Qurbanov,
K.Y. Deqtaryov, N.Ə. İmamverdiyev, N.Ş. İsmayılov, A.D. İsmayılzadə,
J. Kaspşik, A.T. Məmmədov, V. Pedriç, Ç,Q. Rəsulov, N.M. Səfərov,
V.M. Seyidov, E.F. Sultanov, A.İ. Timurziyev, Ə.A. Feyzullayev,
V.M Valyayev, A.V. Yazenin, Ə.Z. Zalov, N.P. Zapivalov

Jurnal Azərbaycan Respublikası Prezidenti yanında Ali Attestasiya Komissiyasının qərarı ilə dissertasiya işlərinin dərc olunduğu nəşrlər siyahısına daxil olunub

N E W S

Of Azerbaijan Higher Technical Educational Institutions

EDITOR-IN-CHIEF: PROFESSOR MUSTAFA BABANLI
Deputy editor-in-chief – Rauf Aliyarov
Responsible secretary – Oleg Huseynov

EDITORIAL BOARD:
V.M. Ahmadov, I.A. Garagash, H.B. Guliyev, R.S. Gurbanov,
K.Y. Degtarev, N.A. Imamverdiyev, N.Sh. Ismayilov, A.D. Ismailzadeh,
J. Kacprzyk, A.T. Mammadov, W. Pedrycz, Ch.G. Rasulov, N.M. Safarov,
V.M. Seidov, E.F. Sultanov, A.I. Timurziev, A.A. Feyzullayev,
V.M. Valyaev, A.V. Yazenin, A.Z. Zalov, N.P. Zapivalov

The journal by decision of Higher Attestation Commission under the President of Azerbaijan Republic is included in the list of scientific editions, in which the results of thesis works publish

И З В Е С Т И Я

Высших технических учебных заведений Азербайджана

ГЛАВНЫЙ РЕДАКТОР: ПРОФЕССОР МУСТАФА БАБАНЛЫ
Заместитель главного редактора – Рауф Алияров
Ответственный секретарь – Олег Гусейнов

РЕДАКЦИОННАЯ КОЛЛЕГИЯ:
В.М. Ахмедов, И.А. Гарагаш, Г.Б. Гулиев, Р.С. Гурбанов,
К.Ю. Дегтярев, Н.А. Имамвердиев, Н.Ш. Исмайлов, А.Д. Исмаилзаде,
Я. Кацпшик, А.Т. Мамедов, В. Педрич, Ч.Г. Расулов, Н.М. Сафаров,
В.М. Сеидов, Э.Ф. Султанов, А.И. Тимурзиев, А.А. Фейзуллаев,
В.М. Вальяев, А.В. Язенин, А.З. Залов, Н.П. Запивалов

Журнал решением Высшей аттестационной комиссии при Президенте Азербайджанской Республики включен в перечень научных изданий, в которых публикуются результаты диссертационных работ

M Ü N D Ə R İ C A T

C O N T E N T S

News of Azerbaijan Higher Technical
Educational Institutions
ISSN 1609-1620
Volume 23, № 5 (2021), 6-9
UDC 622.245

Destruction of wellbore stability due to mechanical effects

Oil and gas

Guluzadeh T.E.
Azerbaijan State Oil and Industry University
Email: tural.quluzadeh@gmail.com

An important condition for the wellbore stability is to maintain a balance between in-situ stresses in the wellbore wall and the strength of the surrounding rock masses. In general, stability in a wellbore is a reaction to the stresses that affect the strength of the surrounding rock mass during drilling. When studying the wellbore stability, it is assumed that the directions of isotropic and in-situ stresses in the rocks are known. However, these assumptions are not true in reality. The state of the initial stress at a certain depth in the ground determines the sum of the stresses around the new hole. Determining this initial condition before exploring a new field helps to drill. If the wellbore is drilled into a bed of soft rocks, such as a layer of poorly cemented sand, the stability of the wellbore will be weakened as a result of the release of previously existing in-situ stresses underground. In order to predict all these cases and to prevent their negative effects, the mechanical review point of the wellbore should be studied in detail.

Keywords: in-situ stress, tangential stress, vibration, creeping, tensile failure.

Introduction

Before a well is drilled into the ground, the rocks are layered as a result of vertical compression and horizontal stresses, as well as lateral pressure. The local stress state can be determined by 3 main stresses: vertical stress (σ_v), maximum horizontal stress (σ_H), and minimum horizontal stress (σ_h). The minimum horizontal stress can be measured by hydraulic fracturing and leak-off tests (Amadei and Stephansson, 1997). Determining the maximum horizontal stress can be guessed only based on specific considerations.

Assume that the rock system is in a state of static equilibrium stress because there is no seismic activity nearby, and there is no movement here. Disturbance of the equilibrium state of stress after drilling the wellbore causes instability in the adjacent rock layer. This condition is more common in “Garadagh” and “Gunashli” fields. The rocks around the wellbore must be able to withstand that weight to re-establish the equilibrium state of the load that the removed rocks continue to carry.

Statement of the problem

Depending on the purpose of drilling, the walls of the drilled well are usually supported by the pressure of the drilling mud. This pressure must prevent the initial slip from reaching the deformation limit of the rock found in the wellbore wall. On the other hand, the pressure of the drilling mud can cause elongation deformation in the wellbore, which can cause hydraulic fracturing [1].

Some factors that disrupt wellbore instability occur when a wellbore is drilled. These are the state of in-situ stresses, the type of well (vertical, inclined), the trajectory of the wellbore, the

parameters of the rocks (strength, permeability, etc.), the shale-mud interaction, and thermal effects. These factors can be grouped as mechanical, chemical, and thermal effects.

Rocks in the depths of the ground are under in-situ stress. The condition of stress is in equilibrium before drilling. During the drilling process, the rocks in the wellbore are replaced with drilling mud. As a result, the distribution of stress around the wellbore changes and if the rock strength is insufficient, the wellbore will collapse (Bradley, 1979) (Figure).

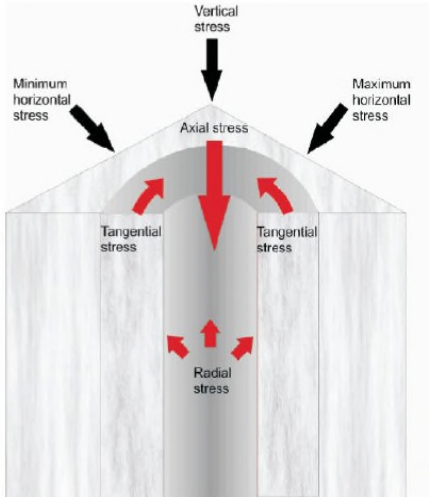

Figure. The conditions of stresses in the wellbore

Solution methods

In the design of a wellbore, it is important to determine the density of the drilling mud that will ensure the stability of the wellbore. The upper limit of the density of the mud is limited by the tension failure. The lower limit is limited by the compression failure. The density of the drilling mud between these two limits is called the safe mud weight window.

The minimum density of the drilling mud must be known to prevent compression deformation in the wellbore during drilling. This is called the "low critical value of the density of the drilling mud". If the density of the drilling mud is lower than this value, the stability of the wellbore will be weakened due to compression deformation. On the other hand, the value of the density of the drilling mud must be less than the tension deformation of the rock. This is called the " upper critical value of the density of the drilling mud" [2].

According to many observations, the wellbore is more stable when the wellbore is drilled perpendicular to the bedrock (Last və b.,1995, Ocland və b.,1998, Beacom və oth., 2001).

Determination of the compressive strength of clay is one of the key factors in regulating the drilling operation, drill bit selection, and wellbore stability.

The effective normal stress (σ_e) is equal to the total normal stress minus the hydraulic pore pressure (Terzagi, 1925):

$$\sigma_e = \sigma_t - P_p \quad (1)$$

Biot (1941) improved this formula by adding the Biot constant, which takes into account the compressive capacity of pore fluid and rock:

$$\sigma_e = \sigma_t - \alpha_p P_p \quad (2)$$

Here $\alpha_p = 1 - \frac{K_{fr}}{K_s}$ Biot constant is the ratio of the change in the volume of the filled pore to the change in the volume of the rock during fluid leaves the rock. K_{fr} is the module of elasticity of fluid extracted rock, N/m^2. The module of elasticity is the inverse of the volume compression ratio. K_s is the module of elasticity of the rock.

Direct and indirect (empirical formulas) methods are used to determine the scale of stresses. Direct methods of stress measurement include hydraulic fracturing, flow, micro-cracking, and

injection testing (Haimson&Fairhurst 1967, Gaarenstroom, Tromp, De Jong&Brandenburg, 1993; Economides, Oligney, & Valko, 2000). Because these tests are expensive and difficult (especially at great depths), they are rarely performed.

Density logging is used to calculate the vertical stress in the wellbore. Geomechanical parameters such as Poisson's ratio, Joung`s modulus, and unilateral compressive strength are calculated using empirical formulas. These formulas are often based on petrophysical data such as compression wavelength slowdown and neutron logging. The results are checked through laboratory data. In vertical wells, the direction of collapsing of the wellbore indicates the direction of the minimum horizontal stress, and the direction of tension failure indicates the direction of the maximum horizontal stress. Repeated touching of the drill pipe to the wellbore increases the tension, which leads to collapse. The effect of this touch can be determined by logging images of the caliper logging. Siphon and swab pressure can also cause the wellbore to collapse [3].

When abnormally pressurized clays are drilled, the pore pressure pulls the clays out of the well wall. Tectonic stressed clays are mainly found in the part of the Earth's crust where tectonic movements took place. In these cases, the layer of clay layering is in the direction of the applied stress. When a wellbore is drilled, this tension causes the collapse of rocks.

The fluidity of rocks is due to the formation of creeping (deformation) in low-permeability rocks (clay, claystone) as a result of the redistribution of pore pressure. Rocks that are relatively permeable and do not show creeps, such as sandstone and limestone, are considered that they are not fluidity. Before drilling, the pore pressure is uniform in the horizontal plane. When a well is drilled, the stresses around the wellbore are redistributed according to the mass of rock drilled, and this is replaced by the pressure of the drilling mud. As the porous fluid moves within the rock, the stresses compensate for the fluid pressure.

During the drilling process, the rock mass is exposed to the pressure of the drilling mud and tectonic stresses. The wellbore is also affected by thermal stresses caused by the temperature difference between the drilling mud and the rock mass.

When the pressure inside the wellbore is less than the pore pressure, the stability is disturbed by a slip or compression stress. When the pressure inside the wellbore exceeds the fracture pressure of the rock, collapse without tension occurs.

There are 3 types of drill pipe vibration: axial, torsional, lateral. The destructive power of each vibration is different. Lateral vibrations are more destructive and cause more shocks to the well wall. As a result, cracks appear in the well wall, which leads to an increase in the diameter of the wellbore. To prevent this, the optimized lower part of the drill pipe must be assembled appropriately to wellbore geometry, curvature, and rocks.

The main factors that have been theoretically determined and affect the mechanical stability of the wellbore are these: 1) in-situ stresses in different layers of rock; 2) mechanical properties of rock; 3) change of pore pressure; 4) density of drilling mud; 5) zenith and azimuth angle; 6) thermal effects; 7) anisotropy.

In order to predict whether a wellbore is stable or unstable, it is important to clarify the in-situ stresses observed in the boreholes drilled in the area. For example, the controlling of stress-induced wellbore instability and the design of inclined and horizontal wells require information on the price and direction of in-situ stresses (Tan and oth.1993). Hydraulic fracturing is the most common method for determining the value of local stress in a wellbore. The analysis of in-situ stresses is based on the determination of compressive and tensile stresses by the electrical and acoustic display (imaging) logging by Bruji and Kjorholt (2011).

Bradley (1979) found that the curvature of the wellbore has a significant effect on the pouring of rocks. As the wellbore curvature increases, more drilling mud pressure is required to ensure the wellbore stability. The direction of the wellbore also plays an important role in the stability of the wellbore (especially in tectonic active areas).

It is impossible to control the in-situ stress conditions, but it is possible to control the direction of the well due to the stresses. The temperature of the drilling mud is reduced to regulate the effect of temperature on the wellbore stability.

Conclusion

1. In the design of the wellbore, the lower and upper critical limits of the mud weight of the drilling mud must be determined due to ensure the wellbore stability. The weight of the drilling mud between these two limits is called the safe mud weight window.

2. When the pressure inside the wellbore is less than the pore pressure, the stability is disturbed by a slip or compression stress.

References

1. Hashemi S. Drilling and maintaining stable unsupported boreholes in poorly cemented sandy formations. / Thesis. – Australia, 2015. – P.90.

2. Han G., Henson J., Timmis A., Abdul Aziz I. Wellbore stability study: Lessons and learnings from a tectonically active field. / National Technical conference & exhibition. – New Orleans, Lousiana. – Pp.1-3.

3. Abdideh M., Alisamir S. Analysis of deep stress field using well log and wellbore breakout data: a case study in cretaceous oil reservoir, Southwest Iran. // Geodesy and Cartography. – 2018. – Vol.44, Issue 4. – Pp.2-3.

Xülasə
Quluzadə T.E.
Mexaniki təsirlərdən quyu lüləsinin davamlılığının pozulması

Quyu lüləsinin davamlılığı üçün vacib şərt quyu divarında yerli gərginliklər və əhatə olunmuş süxur kütlələrinin möhkəmliyi arasındakı tarazlığı saxlamaqdır. Ümumiyyətlə, quyu lüləsində davamlılıq qazıma zamanı əhatə olunmuş süxur kütləsinin möhkəmliyinin təsir edən gərginliklərə qarşı reaksiyasıdır. Quyu lüləsinin davamlılığını tədqiq edərkən süxurların izotrop və yerli gərginliklərinin istiqamətlərinin məlum olması fərz olunur. Lakin bu fərziyələr reallıqda doğru deyil. Yerin dərinliyində müəyyən dərinlikdə ilkin gərginliyin vəziyyəti yeni lülənin ətrafındakı gərginliklərin cəmini müəyyən edir. Yeni yatağın kəşfiyyatından əvvəl bu ilkin vəziyyətin təyin olunması qazma işlərinə kömək edir. Quyu lüləsi zəif sementlənmiş qum layı kimi yumşaq süxurlar olan laya qazılarsa, yer altında əvvəl mövcud olan yerli gərginliklərin azad olması nəticəsində quyu lüləsinin dəyanətliliyi pozulur. Bütün bu qeyd olunan halları proqnozlaşdırmaq və mənfi təsirlərin qarşısını almaq üçün quyu lüləsi mexaniki nöqteyi-nəzərdən ətraflı tədqiq olunmalıdır.

Açar sözlər: yerli gərginlik, tangensial gərginlik, vibrasiya, sürüngənlik, dartınmadan dağılma.

News of Azerbaijan Higher Technical
Educational Institutions
ISSN 1609-1620
Volume 23, № 5 (2021), 10-15
UDC 549.67: 544.47: 542.941.8

Kinetic modeling of the oxidative dehydrogenation of cyclopentane over modified zeolites

Chemistry and chemical technology

Shabanova Z.A.
Oil and Gas Scientific Research Project Institute, SOCAR
E-mail: zumrud-042425-@mail.ru

The kinetics and mechanism of the oxidative dehydrogenation of cyclopentane with the participation of molecular oxygen on a modified zeolite catalyst have been studied. A theoretically substantiated kinetic model of the process has been developed. The numerical values of the kinetic and adsorption parameters have been determined, which make it possible to describe the experimental data within the error of quantitative analysis. Kinetic experiments were carried out in the temperature range 350-390^{0}C, space velocity 500-2500 h^{-1}, and at various partial pressures of the reagents. The optimal parameters of the reaction of oxidative dehydrogenation of cyclopentane to cyclopentadiene have been determined.

Keywords: kinetics, mechanism, oxidative dehydrogenation, zeolite catalyst.

Introduction

One of the perspective areas for the production of cyclic unsaturated hydrocarbons is one-stage catalytic conversion of naphthenic hydrocarbons. The most widely studied is the reaction of catalytic dehydrogenation of naphthenic hydrocarbons in an absence of oxygen [1, 2]. It is known that this is a thermodynamically limited reaction, carried out under harsh conditions, leading to aromatization and resinification of a significant part of the hydrocarbon fraction, as well as rapid coking and deactivation of the catalysts used. The use of molecular oxygen as hydrogen acceptors allows the process to be carried out under milder conditions and to prevent the above mentioned complications.

Statement of the problem

In previous works [3-5], we found that narrow-pore zeolites modified with metal cations by ion exchange exhibit relatively high catalytic activity and selectivity in the reactions of oxidative conversion of cyclohexane hydrocarbons at relatively low temperatures (250-350^{0}C).

In light of the above, it became necessary to conduct systematic studies on the oxidative dehydrogenation of cyclopentane in the presence of modified forms of narrow-pore zeolites.

Solution methods

The oxidative dehydrogenation of cyclopentane was carried out on modified narrow-pore zeolite catalysts selected on the basis of a previously conducted search, in the temperature range of 300-500^{0}C, a feed space velocity of 1000-3000 h^{-1} and a molar ratio of cyclopentane: O_2 = 1: 0.1-1 at atmospheric pressure. It was found that cyclopentane under the above conditions undergoes

transformation in the following directions: dehydrogenation, disproportionation of hydrogen atoms, cracking and deep oxidation. The main directions of these transformations are the dehydrogenation of the starting hydrocarbon. At 300-350^{0}C dehydrogenation of cyclopentane mainly competes with deep oxidation of hydrocarbons. With an increase in temperature to 450^{0}C, the selectivity of the reaction with respect to cyclopentadiene slightly increases, however, an intensification of other side reactions is observed. It was found that natural clinoptilolite containing cations Cu^{2+} – 0.5 wt.%, Zn^{2+} – 0.2 wt.%, Co^{2+} – 0.1 wt.% and Cr^{3+} – 0.1 wt.%, is an active catalyst for reactions of oxidative dehydrogenation of cyclopentane to cyclopentene and cyclopentadiene [6].

The results of an experimental study of the kinetic regularities of the oxidative dehydrogenation of cyclopentane on an active catalyst are presented in Table 1. Kinetic experiments were carried out in the temperature range 350-390^{0}C, space velocity 500-2500 h^{-1}, and at various partial pressures of the reagents.

Table 1. Results of kinetic experiments of the oxidative dehydrogenation of cyclopentane on the CuZnCoCr-clinoptilolite catalyst

Partial pressure of reagents, atm.		Space velocity, $ч^{-1}$	Temperature, ^{0}C	Cyclopentane conversion, %	The yield of reaction products,%		
$P_{C_5H_{10}}$	P_{O_2}				C_5H_8	C_5H_6	CO_2
0.2738	0.1540	2000	320	6.6	1.8	3.9	0.9
0.2738	0.1540	2000	340	8.2	0.7	5.1	2.4
0.2738	0.1540	2000	360	11.9	3.2	5.5	3.2
0.2738	0.1540	2000	380	13.6	3.7	6.3	3.6
0.2738	0.1540	2000	390	25.3	2.5	8.8	14.0
0.2980	0.1489	1000	320	19.8	14.7	3.2	1.9
0.2980	0.1489	1000	400	11.7	2.1	7.0	2.6
0.2980	0.1489	1000	350	11.0	1.1	3.3	6.6
0.2980	0.1489	1000	370	12.3	2.8	5.1	4.4
0.2980	0.1489	1000	390	13.4	3.8	6.6	3.0
0.2980	0.1489	1000	380	9.4	2.5	5.7	1.2
0.3225	0.0768	500	390	14.8	0.8	5.6	8.4
0.5641	0.1491	2500	370	13.1	6.6	4.9	1.6
0.5641	0.1491	2500	390	15.4	15.4	7.3	3.1

From the experimental data, it was confirmed that the kinetic scheme of the considered reaction through the active catalytic system does not proceed according to a sequential mechanism. From these experimental data, it can be concluded that various active sites appear on the catalyst surface, which are responsible for the formation of reaction products. The mechanism of the oxidative dehydrogenation of cyclopentane at the aforementioned active sites can be represented as the following scheme of steps:

$$O_2 + 2Z_1 \xrightarrow{k_1} 2Z_1O \qquad \frac{1}{2}$$

$$O_2 + 2Z_2 \xrightarrow{k_2} 2Z_2O \qquad \frac{1}{2}$$

$$(Z_1O + Z_2O) + C_5H_{10} \xrightarrow{k_3} (Z_1O + Z_2O)C_5H_{10} \qquad 1$$

$$(Z_1O + Z_2O)C_5H_{10} \xrightarrow{k_4} C_5H_6 + 2H_2O + Z_1 + Z_2 \qquad 1$$

$$C_5H_{10} + O_2 = C_5H_6 + 2H_2O$$

We can write the following expressions for the stage rates:

$$r_1 = k_1\theta_1^2 P_{O_2},\ r_2 = k_2\theta_2^2 P_{O_2},\ r_3 = k_3\theta_3 P_{C_5H_{10}},\ r_4 = k_4\theta_4$$

Under stationary conditions:

$$r = r_1 = r_2 = r_3 = r_4,$$

where θ_1, θ_2, θ_3 и θ_4 – fractions of free areas of the catalyst surface capable of adsorbing oxygen, covered with atomic sorption oxygen and cyclopentane molecules.

$$\theta_4 = \frac{k_3\theta_3 P_{C_5H_{10}}}{k_4}\ \theta_1 = \sqrt{\frac{k_3 P_{C_5H_{10}}}{k_1 P_{O_2}}}\ \sqrt{\theta_3}\ \theta_2 = \sqrt{\frac{k_3 P_{C_5H_{10}}}{k_2 P_{O_2}}}\ \sqrt{\theta_3},$$

$$\theta_1 + \theta_2 + \theta_3 + \theta_4 = 1,$$

$$\frac{k_3 P_{C_5H_{10}}}{k_4}\theta_3 + \left(\sqrt{\frac{k_3 P_{C_5H_{10}}}{k_1 P_{O_2}}} + \sqrt{\frac{k_3 P_{C_5H_{10}}}{k_2 P_{O_2}}}\right)\sqrt{\theta_3} - 1 = 0.$$

By designating

$$\frac{k_3 P_{C_5H_{10}}}{k_4} = A,\ \left(\sqrt{\frac{k_3 P_{C_5H_{10}}}{k_1 P_{O_2}}} + \sqrt{\frac{k_3 P_{C_5H_{10}}}{k_2 P_{O_2}}}\right) = B,\ \theta_3 = x^2,\ \sqrt{\theta_3} = x$$

We get

$$Ax^2 + Bx - 1 = 0$$

$$x = \frac{-B + \sqrt{B^2 + 4A}}{2A}$$

$$\theta_3 = x^2 = \left\{\frac{-B + \sqrt{B^2 + 4A}}{2A}\right\}^2$$

Then, the equation for the formation rate of 1,3-cyclopentadiene will take the form

$$r = r^1_{C_5H_6} = k_3 P_{C_5H_{10}} \cdot \left\{\frac{-B + \sqrt{B^2 + 4A}}{2A}\right\}^2$$

$$r = r^1_{C_5H_6} = k_3 P_{C_5H_{10}} \cdot \left\{\frac{-\left(\sqrt{\frac{k_3 P_{C_5H_{10}}}{k_1 P_{O_2}}} + \sqrt{\frac{k_3 P_{C_5H_{10}}}{k_2 P_{O_2}}}\right) + \sqrt{\left(\sqrt{\frac{k_3 P_{C_5H_{10}}}{k_1 P_{O_2}}} + \sqrt{\frac{k_3 P_{C_5H_{10}}}{k_2 P_{O_2}}}\right)^2 + 4\frac{k_3 P_{C_5H_{10}}}{k_4}}}{2\frac{k_3 P_{C_6H_{12}}}{k_4}}\right\}^2 \quad (8.1)$$

The stage diagram of the mechanism of formation of cyclopentene can be represented as follows:

$O_2 + 2Z_3 \xrightarrow{k_5} 2Z_3O$	$\frac{1}{2}$
$Z_3O + C_5H_{10} \xrightarrow{k_6} Z_3OC_5H_{10}$	1
$Z_3OC_5H_{10} \xrightarrow{k_7} C_6H_8 + H_2O + Z_3$	1

$$C_5H_{10} + 1\frac{1}{2}O_2 = C_5H_8 + H_2O$$

Expressions for stage rates

$$r_5 = k_5\theta_5^2 P_{O_2}, \quad r_6 = k_6\theta_6 P_{C_5H_{10}}, \; r_7 = k_7\theta_7 .$$

Under stationary conditions:

$$r = r_5 = r_6 = r_7,$$

where θ_5, θ_6, и θ_7 – fractions of free areas of the catalyst surface capable of adsorbing oxygen, covered with atomic-sorption oxygen and cyclopentane molecules;

$$\theta_5 + \theta_6 + \theta_7 = 1$$

$$\theta_7 = \frac{k_6 P_{C_5H_{10}}}{k_7}\theta_4, \; \theta_5 = \sqrt{\frac{k_6 P_{C_5H_{10}} \cdot \theta_4}{k_5 P_{O_2}}},$$

$$\frac{k_6 P_{C_5H_{10}}}{k_7}\theta_6 + \theta_4 + \sqrt{\frac{k_6 P_{C_5H_{10}}}{k_5 P_{O_2}}}\sqrt{\theta_6} - 1 = 0 .$$

By designating

$$\frac{k_6 P_{C_5H_{10}}}{k_7} + 1 = c, \; \sqrt{\frac{k_6 P_{C_5H_{10}}}{k_5 P_{O_2}}} = d, \; \theta_6 = x^2, \; \sqrt{\theta_6} = x,$$

We get

$$cx^2 + dx - 1 = 0$$

$$x = \frac{-d + \sqrt{d^2 + 4c}}{2c},$$

$$\theta_{11} = x^2 = \left\{\frac{-d + \sqrt{d^2 + 4c}}{2c}\right\}^2 .$$

$$cx^2 + \mathrm{d}x - 1 = 0$$

$$\theta_6 = x^2 = \left\{\frac{-d + \sqrt{d^2 + 4c}}{2c}\right\}^2$$

Then the equation for the rate of formation of cyclohexene takes the form

$$r = r^1_{C_5H_8} = k_6 P_{C_5H_{10}} \cdot \left\{\frac{-d + \sqrt{d^2 + 4c}}{2c}\right\}^2,$$

$$r = r^1_{C_5H_8} = k_6 P_{C_5H_{10}} \cdot \left\{\frac{-\sqrt{\frac{k_6 P_{C_5H_{10}}}{k_5 P_{O_2}}} + \sqrt{\left(\sqrt{\frac{k_6 P_{C_5H_{10}}}{k_5 P_{O_2}}}\right)^2 + 4\left(\frac{k_6 P_{C_5H_{10}}}{k_7} + 1\right)}}{2\left(\frac{k_6 P_{C_5H_{10}}}{k_7} + 1\right)}\right\}^2 \quad (8.2)$$

Suppose CO_2 is formed by the interaction of adsorbed molecules of cyclopentane, cyclopentene and cyclopentadiene-1,3 with adsorbed oxygen molecules. Kinetic equations corresponding to these mechanisms:

$$r^1_{CO_2} = \frac{k_8 K_1 P_1 K_6 P_2}{\left(1 + K_1 P_1 + \sqrt{K_2 P_2} + K_3 P_3 + K_4 P_4 + K_5 P_5\right)^2} \quad (8.3)$$

$$r^2_{CO_2} = \frac{k_9 K_3 P_3 K_6 P_2}{\left(1 + K_1 P_1 + \sqrt{K_2 P_2} + K_3 P_3 + K_4 P_4 + K_5 P_5\right)^2} \quad (8.4)$$

$$r_{CO_2}^3 = \frac{k_{10}K_4P_4K_6P_2}{\left(1+K_1P_1+\sqrt{K_2P_2}+K_3P_3+K_4P_4+K_5P_5\right)^2} \quad (8.5)$$

$$r_{C_5H_8} = r_{C_5H_8}^1 - r_{CO_2}^2 \quad (8.6)$$

$$r_{C_5H_6} = r_{C_5H_6}^1 - r_{CO_2}^3 \quad (8.7)$$

$$r_{CO_2} = r_{CO_2}^1 + r_{CO_2}^2 + r_{CO_2}^3 \quad (8.8)$$

Equations (8.6) - (8.8) constitute the kinetic model of this reaction.

The developed kinetic model of the reaction was subjected to statistical analysis based on kinetic data. The calculated numerical values of the constants of the kinetic model are presented in Table 2.

Table 2. Numerical values of the kinetic model constants

$\ln k_i^0 (\ln K_i^0)$		$E_i(Q_i)$, ккал/моль	
$\ln k_1^0$	53.89	E_1	20.62
$\ln k_2^0$	86.76	E_2	19.76
$\ln k_3^0$	3.62	E_3	23.48
$\ln k_4^0$	20.81	E_4	20.56
$\ln k_5^0$	61.88	E_5	19.88
$\ln K_1^0$	-16.43	Q_1	5.05
$\ln K_2^0$	-49.30	Q_2	4.50
$\ln K_3^0$	-21.34	Q_3	7.25
$\ln K_4^0$	-61.23	Q_4	10.0
$\ln K_5^0$	-33.49	Q_5	2.26

Calculations showed that the relative discrepancy between the experimental and calculated data did not exceed 10-15%.

Conclusion

The catalytic activity of a number of ultradispersed multicomponent metal-zeolite catalysts synthesized on the basis of a natural zeolite, clinoptilolite, and metal cations was studied in the reaction of vapor-phase oxidative dehydrogenation of cyclopentane with molecular oxygen into the corresponding diene. It was found that natural clinoptilolite containing cations Cu2+ – 0.5 wt.%, Zn2+ – 0.2 wt.%, Co2+ – 0.1 wt.% and Cr3+ – 0.1 wt.%, is an active catalyst for reaction of oxidative dehydrogenation of cyclopentane to cyclopentene and cyclopentadiene. On the basis of experimental data it has been established kinetic scheme of the reaction. It has been developed theoretically based kinetic model of the process. The numerical values of the constants of the kinetic equation have been calculated.

References

1. Coughlan, B., Keane, M.A. The catalytic dehydrogenation of cyclohexane and methylcyclohexane over nickel loaded Y zeolites. // Catal. Lett 5. –1990. – Pp.89-100. doi:10.1007/BF00763942

2. Laila I., Alia Abdel-Ghaffar A., Alia S.M. Dehydrogenation of cyclohexane on catalysts containing noble metals and their combinations with platinum on alumina support. // Applied Catalysis A: General. – 1999. – Vol. 177 (1). – Pp.99-110. doi.org/10.1016/S0926-860X(98)00248-8

3. Алиев А.М., Шабанова З.А., Наджаф-Кулиев У.М. Окислительное дегидрирование циклогексана на модифицированных цеолитных катализаторах. // Нефтехимия. – М., 2016, №4. – С. 407-415. http://neftekhimiya.ips.ac.ru

4. Алиев А.М., Шабанова З.А., Керимов А.И. Синтез и исследование цеолитов, модифицированных катионами металлов, в качестве катализаторов в реакции окислительного дегидрирования нафтеновых углеводородов. // Журнал прикладной химии. – 2017. – Т.90. – Вып. 5. – С.591-597.

5. Алиев А.М., Шабанова З.А., Керимов А.И. Селективное окислительное дегидрирование метилциклогексана на модифицированных цеолитных катализаторах. // Нефтепереработка и нефтехимия. – М., 2018, №2. – С.40-48. http://www.npnh.ru

6. Aliyev A.M., Abbasov M.Y., Shabanova Z.A., Ali-zadeh G.A., Najaf-Guliyev U.M. A study of the kinetics and mechanism of the selective oxidative dehydrogenation reaction of cyclopentane to cyclopentadiene-1,3 over modified zeolite catalysts. // Azerb. Chem. Journal. – 2018, №3. – Pp.64-72.

Xülasə

Şabanova Z.A.

Modifikasiya olunmuş seolit katalizatoru üzərində tsiklopentanın oksidləşdirici dehidrogenləşməsinin kinetik modelləşdirilməsi

Modifikasiya olunmuş seolit katalizatoru üzərində molekulyar oksigen iştirakında tsiklopentanın oksidləşdirici dehidrogenləşməsinin kinetikası və mexanizmi öyrənilmişdir. Prosesin kinetik qanunauyğunluqları 350-390^{0}C temperatur, 500-2500 saat-1-həcmi sürət intervalında və reagentlərin müxtəlif parsial təzyiqlərində öyrənilmişdir. Tsiklopentanın tsiklopentadienə selektiv oksidləşdirici dehidrogenləşməsi reaksiyasının optimal parametrləri müəyyən olunmuşdur. Prosesin nəzəri cəhətdən əsaslandırılmış kinetik modeli işlənib hazırlanmışdır. Miqdari analizin yolverilən xəta həddində təcrübi nəticələri təsvir etməyə imkan verən kinetik parametrlərin ədədi qiymətləri təyin olunmuşdur. Eksperimental və hesablanmış məlumatlar arasındakı nisbi xətanın 10-15% -dən az olması müəyyən olunmuşdur.

Açar sözlər: kinetika, mexanizm, oksidləşdirici dehidrogenləşmə, seolit katalizatoru.

News of Azerbaijan Higher Technical
Educational Institutions
ISSN 1609-1620
Volume 23, № 5 (2021), 16-20
UDC 628.547

Hydrogenation of the light pyrolysis resin via the presence of catalyst “over surface of nickel kiselgur”

Chemistry and chemical technology

Ibadova R. S., Huseynova E.A.
Azerbaijan State Oil and Industry University
E-mail: ibadova.reyhan@gmail.com

Hydrogenation of a light pyrolysis resin via the presence of catalyst “over surface of nickel kiselgur” has been carried out.The physico-chemical properties of the obtained samples were investigated. In the result of conducted analysis it has been determined that by realivation of process during 60 minutes by 100ºC the hydrogenation degree of undesirable desaturated hydrocarbons makes up 94,9% and the hidrogenate considered concentrate of C_7-C_8 aromatic hydrocarbons. The amount of hydrocarbons was determined by chromatography. The dehydrogenation of the obtained naphthenic hydrocarbons to aromatic hydrocarbons as well as the hydrogenation to unsaturated hydrocarbons indicates the high activity of the catalyst. Normal paraffins and naphthalene had proved the activity of the catalyst in destructive hydrocracking reactions. The residues can be used to obtain individual hydrocarbons (naphthene, benzene) and raw materials for the organization.

Keywords: light pyrolysis resin, catalyst “over surface of nickel kiselgur”, hydrogenation, aromatic hydrocarbons.

Introduction

Pyrolysis is a more severe thermal cracking of oil and gas feedstocks. The process is carried out at a temperature of 700-900ºC. The purpose of this process is to obtain gaseous hydrocarbons rich in olefins [1-3].

In the pyrolysis process, the maximum amount of ethylene, propylene, butadiene, butylene, etc. can be obtained by choosing the right mode. In this process, some liquid products and resins are obtained along with gaseous hydrocarbons. They contain resins containing monocyclic (benzene, toluene, xylenols) and polycyclic aromatic hydrocarbons. Olefins – rich gaseous hydrocarbons are the target product in the pyrolysis process. Ethylene occupies the main place among these hydrocarbons.

When liquid products are rectified, four fractions are obtained. C_5-70ºC, 70-130ºC (benzene, toluene) fraction 130-190ºC (C_8-C_9) and above 190ºC (heavy resin olefins) contain up to 50% cyclopentadiene and isoprene [4-6], which is a high reaction pesticides, plasticizers are obtained on the basis of it. Isoprene is one of the best monomers for obtaining synthetic rubber, xylene and ethylene benzene are significant styrene and other alkenylaromatic hydrocarbons

Light pyrolysis resin contains a certain amount of aromatic hydrocarbons, which can be used as a valuable raw material for organic synthesis [7-10]. There is a traditional scheme of processing and application of pyrocondensate. Previously, it was subjected to selective hydrogenation in the presence of palladium alumina catalyst. The main goal here was to remove chemically unstable diene and vinylaromatic compounds. It was also used as a gasoline component. However, in January 1999,

with the introduction of new standards for the amount of gasoline (≤5.0%), the introduction of hydro-stabilized pyrocondensate in addition to hydrostabilized pyrocondensate was considered appropriate, mainly because of the demand for benzene as a commodity.

Currently, pyrocondensate is divided into three parts: C_5, C_6, C_8, C_9, which are subject to hydrostabilization. The streams C_5 and C_9 are then used as high-molecular gasoline, but the C_6-C_8 fraction is sent for hydrotreating and then for hydrodealkylation to obtain benzene. In recent years, in the processing of pyrocondensate and its fractions is used catalyst APKQS-20E1, developed by specialists of Alvigo-M LLC. This catalyst is applied in a thin layer over the clay carrier [10].

Heavy pyrolysis resin has also been studied with palladium. For heavy pyrolysis resins, it was applied with a "nickel over a kiselgur" catalyst [11]. The properties of the naphthalene fraction were considered by the authors, developed by industrial analysis. The naphthene fraction with a boiling point of 185ºC is obtained in a two-stage hydrogenation fraction. This fraction can be used as a component of jet or diesel fuels.

The purpose of the applied work is to study the process of hydrogenation of light pyrolysis resin with the catalyst "nickel over kiselgur".

Statement of the problem

Hydrogenation was carried out in a bubble-type device at a pressure of 1 horsepower and a temperature of 80-100ºC. Light pyrolysis resin was used as raw material (density 0.82 g/sm^3, boiling point 40º C). Consumption of hydrogen is 500 l / l of raw material.

As a catalyst, the catalyst "nickel over kiselgur" (TU 2172-033-73776139-2015) was used (cylinder 5 mm in diameter, 6 mm high). 10 gr3 catalyst was taken for each experiment.

4 examples from the presented work were discussed:

– sample 1- primary raw material;

– the sample was processed at 100ºC for 2-60 minutes;

– the sample was processed for 3-120 minutes at a temperature of 100ºC;

– the sample was processed for 4-120 minutes at a temperature of 80ºC.

A number of physicochemical methods of the samples were studied. The amount of hydrocarbons was determined by high-efficiency chromatography.

Prior to the investigation, the catalyst was preheated to 200ºC and activated in a hydrogen stream for 2 h.

Fig.1 shows the distribution of the hydrocarbon group in the samples studied. In Example 1, 50% monoaromatic hydrocarbons, 17% n-paraffin, 17% olefin, 8% naphthene, 4% isoparaffin, 4% polyaromatic hydrocarbons are given in the raw material.

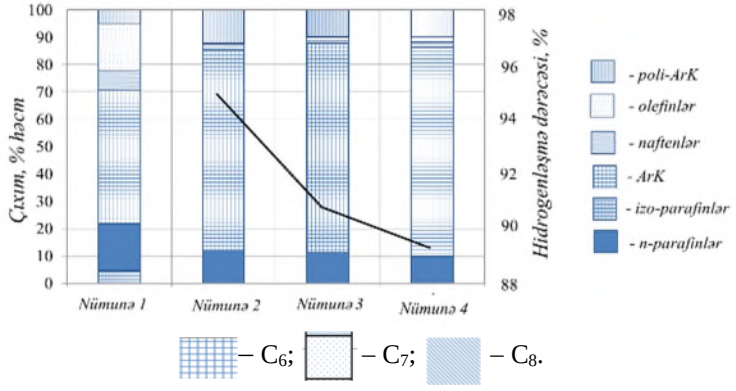

Fig.1. Distribution and degree of hydrogenation of hydrocarbon groups.

After the experiment, the composition of hydrocarbons changed. In Example 2, at a temperature of 100 ° C for 60 minutes, the percentage of monoaromatic hydrocarbons based on the raw material increased from 50% to 74%, and that of polyaromatic hydrocarbons increased from 5% to 12%. With increasing time, the amount of monoaromatic hydrocarbons in sample 3 was 77% at 120°C and 100°C. In Sample 4, the content of monoaromatic hydrocarbons was 77% at 120 minutes at 80ºC.

However, the amount of n-paraffin decreased from 17% to 13% in sample 2, 11% in 3 and 10% in 4. In Example 4, the change was very small in the experiment performed at 80°C for 120 minutes.

The dehydrogenation of naphthenic hydrocarbons to aromatic hydrocarbons and hydrogenation to unsaturated hydrocarbons, as well as the destructive hydrocracking reactions of *n*-paraffins and naphthalene on the hydrocarbon content of the samples, demonstrate the high activity of the catalyst (Fig.1).

Solution methods

These features affect the process parameters and samples taken (Table). Thus, the yield of 78-86% liquid catalyst is associated with the formation of large amounts of low-molecular destructive products, and an increase in the amount of aromatic hydrocarbons leads to an increase in molecular weight. According to the research method, the initial samples differ from the previous samples depending on the high octane number of the samples during the hydrogenation process, according to the engine of an average of 7-13 points. The latter is observed to some extent with an increase in the amount of aromatic hydrocarbons C_7-C_8 against the background of a 2-fold decrease in C_6.

Table. Physical indicators of trials taken with the participation of "nickel over kiselgur"

Indicators	Examples			
	1	2	3	4
Density , q/sm^3	0,786	0,847	0,849	0,849
Molecular mass,q/mol	92,58	106,48	104,91	101,89
Saturated vapor pressure, kPa	44,46	7,24	8,01	10,62
Output, %	–	80	78	86
Octane number: by motor method by investigation method	 86,41 99,85	 93,25 112,67	 93,06 112,17	 91,94 110,94

The fractional composition of all samples is explained in Fig.2. In Example 1, the starting point for the raw material is 40^{o}C, 99.9^{o}C 50%, and the fraction ends at 295.2^{o}C.

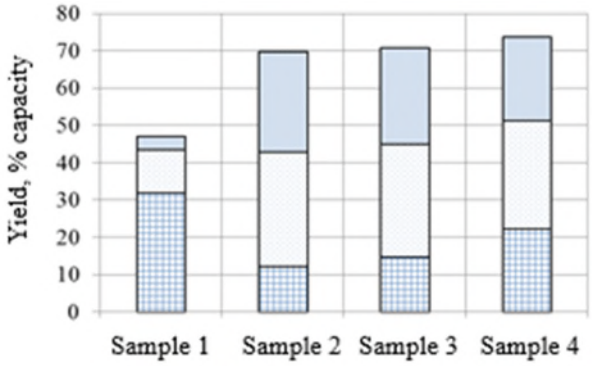

Fig.2. Yield of aromatic hydrocarbons

During the study, the beginning and end temperatures of the fractions obtained from the hydrogenation of light pyrolysis resin are higher than those of the raw material. In Example 2, the boiling point is 87.5^{o}C, the 50% product is 129.2^{o}C and the final temperature is 341.1^{o}C. 120 minutes at 100^{o}C, ie sample 3 is close to trial 2. Thus, the boiling point was 82.3^{o}C, 50% at 127.8^{o}C, and the final temperature was 310.6^{o}C. In Sample 4, ie at 80°C for 120 minutes, the values are lower than in trials 2 and 3. The boiling point was 87^{o}C, 50% at 119.3^{o}C, and the final temperature was 334.9^{o}C.

The fractional composition of trials of light pyrolysis resin obtained during hydrogenation is shown in Fig.3. The 90% fraction boils at gb-180^{o}C, which makes it possible to recommend their gasoline fraction components, and the residues can be used in the production of individual hydrocarbons (naphthene, benzene) and raw materials for the organization.

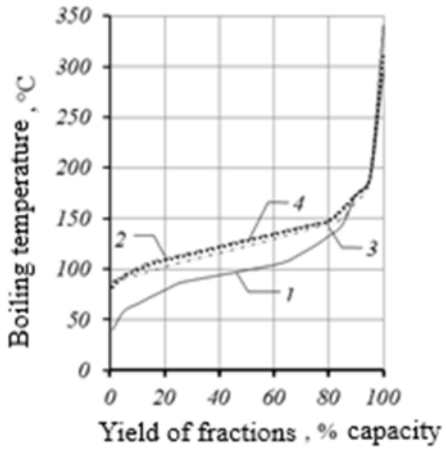

Fig.3. Influence of conditions of hydrogenation process on fraction composition:
1 – Example 1; 2 – Example 2; 3 – Example 3; 4 – Example 4

Conclusion

The results of the researches exposed that, taking into account the resemblance of the physical and chemical characteristics of samples 2 and 4, the degree of hydrogenation of unsaturated hydrocarbons and the amount of benzene were designated to determine the optimal hydrogenation of light pyrolysis resin. The best performance was publicized in Example 2, which was hydrogenated at 100°C for 60 min. Thus, the body of evidence obtained during the hydrogenation of light pyrolysis resin via the presence of a catalyst "nickel over kiselgur" shows that the hydrogenation of unsaturated hydrocarbons reaches 94.4% during the process at 100^{o}C for 60 minutes, and the resulting hydrogenate is aromatic C_7-C_8 is considered a concentrate of hydrocarbons (amount 60.1% by volume).

References

1. Mukhina T.N., Baranov N.L., Babash S.E. and oth. Pyrolysis of hydrocarbons. – M.: Chemistry, 1987. – 240 p.

2. Yampolskiy Yu.P. Elementary reactions and mechanism of hydrolysis of hydrocarbons – M.: Chemistry, 1990. – 216 p.

3. Safarov K.I., Mammadov A.S. Oil and gas refining technology. – Baku, 2000. – 464 p.

4. Berents A.D., Vol-Epstein A.B., Mukhina T.N., Avrekh G.L. Processing of liquid pyrolysis products. – M.: Chemistry, 1985. – 216 p.

5. Lebedeva M.A., Mashukov V.I., Golushko A.K. Analysis and processing of heavy resin pyrolysis. // Chemistry in the interests of sustainable development. – 2012, 20. – Pp.633-638.

6. Mukhamedzyanova A.A., Gimaev R.N., Haybullin A.A., Telyashev E.G. Research of qualitative characteristics of heavy pyrolysis resins. // Bulletin of the Bashkir University. – 2012. – Vol.17, №2. – Pp.902-915.

7. Ahmedova N.F., Mamedov S.E. Complex processing of heavy resin pyrolysis. // Journal of Success of Modern Natural Science. – 2011, №7. – C.74-75.

7. Sokolov V.Z., Kharlampovich G.D. Production and use of aromatic hydrocarbons. – M.: Chemistry, 1980. – 336 p.

8. Bondaletov V.G., Bondaletova L.I., Bondaletov O.V., Sinyavina T.V. Liquid pyrolysis products of hydrocarbons in the synthesis of modified petroleum polymer resins. // Petroleum and petrochemistry. – 2012, №8. – C.24-28.

9. Turkova T.V., Agaronov V.S. and eth. Study of changes in the composition of pyrocondensate and its fractions in the process of selective hydrogenation in the presence of catalysts APKGS series. // Catalysis in industry. – 2005, №4. – Pp.36-41.

10. Akhmetov A.F., Akhmetov A.V., Shaizhanov N.S., Zagidulin Sh.G. Hydroprocessing of the remaining fractions of the pyrolysis process. // Bashkir Chemical Journal. – 2017. – Vol.24, №2. – Pp.4-7.

Xülasə
İbadova R.S., Hüseynova E.Ə.
Yüngül piroliz qatranının "nikel kizelqur üzərində" katalizatorunun iştirakı ilə hidrogenləşməsi

Yüngül piroliz qatranının "nikel kizelqur üzərində" katalizatorun iştirakı ilə hidrogenləşməsi aparılmışdır. Alınan nümunələrin bir sıra fiziki-kimyəvi üsulları öyrənilmişdir. Təcrübədən alınmış nümunlərin analiz nəticələrindən müəyyən olunub ki, 60 dəqiqə müddətində 100^oC-də prosesin aparılması zamanı arzuolunmaz doymamış karbohidrogenlərin hidrogenləşmə dərəcəsi 94.9%-ə çatmış və alınmış hidrogenizat isə C_7-C_8 aromatik karbohidrogen konsentratı hesab edilir. Xromatoqrafiya üsulunun köməyi ilə karbohidrogenlərin aromatik karbohidrogenlərə dehidrogenləşməsi, eləcə də doymamış karbohidrogenlərə hidrogenləşməsi katalizatorun yüksək aktivliyini göstərir. N-parafinlər və nafttalinlər destruktiv hidrokrekinq reaksiyalarında katalizatorun aktivliyini sübut edir. Yüngül piroliz qatranının nümunələri hidrogenləşmə zamanı 90% fraksiyası komponentlərin tövsiyəsinə imkan verir. Qalıqları isə fərdi karbohidrogenlərin (naften, benzol) və qurum üçün xammal alınmasında istifadə oluna bilər.

Açar sözlər: yüngül piroliz qatranı, "nikel kizelqur üzərində" katalizatoru, hidrogenləşmə, aromatik karbohidrogen.

News of Azerbaijan Higher Technical
Educational Institutions
ISSN 1609-1620
Volume 23, № 5 (2021), 21-25
UDC 544.31:546.57.81'23

X-ray study of phase equilibria of the Cu_3SbSe_4-$SnSe_2$ system

Chemistry and chemical technology

Ismayilova E.N.
M.Nagiyev Institute of Catalysis and Inorganic Chemistry, NAS of Azerbaijan
E-mail: Ismayilova818@mail.ru

Phase equilibria in the Cu_3SbSe_4-$SnSe_2$ section of the Cu-Sn-Sb-Se system were studied by differential thermal analysis and powder X-ray diffraction method (PXRD). It was found that in the system the Cu_3SbSe_4 based solid solutions with Sb→Sn substitution (α-phase) are formed. The extent of solid solutions is up to 20 mol %. In the $SnSe_2$-rich region phase equilibria are complex. The phase compositions of the alloys in the entire range of compositions of the investigated section were determined by the PXRD method: α+Cu_2SnSe_3+Sb_2Se_3+Se (20-58 mol.% $SnSe_2$); Cu_2SnSe_3+Sb_2Se_3+Se (60 mol.% $SnSe_2$); Cu_2SnSe_3+ +Sb_2Se_3+$SnSe_2$+Se (more than 60 mol% $SnSe_2$).

Keywords: copper-based chalcogenides, phase equilibria, system, copper-antimony selenide, solid solutions.

Introduction

Copper based chalcogenides are one of the most widely studied semiconductor materials with a variety of functional properties that can be used in several potential applications [1-8]. Recently, synthetic analogs of copper minerals have attracted more attention of researchers, thanks to widespread inexpensive and non-toxic constituents, as well as high thermoelectric properties [9-13]. One of the ways to increase the thermoelectric figure of merit is to doping the known phases with thermoelectric properties with appropriate dopants. So, recent studies have shown that replacing antimony (Sb^{5+}) with low-valence elements such as IIIA and IVA in Cu_3SbSe_4 compound, which is a synthetic analogue of the mineral famatinite, significantly increases the hole carriers concentration and electrical conductivity, resulting in increased thermoelectric efficiency [14-20].

Statement of the problem

The aim of this work was to search and study solid solutions based on the Cu_3SbSe_4 compound with Sb→Sn substitution along the Cu_3SbSe_4-$SnSe_2$ section of the Cu-Sn-Sb-Se system.

This work is part of our comprehensive studies of complex systems based on copper chalcogenides, in which new phases of variable composition were discovered [21-23].

Initial compounds of the title system were investigated in detail. Cu_3SbSe_4 melts congruently at 755 K and has the tetragonal lattice structure of famatinite with parameters: a = = 5,661 Å and c = 11,280 Å [24]. Tin diselenide melts with an open maximum at 920 K [25] and has a hexagonal layered structure (Sp. gr. P-3m1) with following lattice parameters: a = 3.8 Å and c = = 6.13 Å [26].

Solution methods

For the experiments, the initial compounds Cu_3SbSe_4 and $SnSe_2$ were synthesized by fusion of simple substances in stoichiometric ratios in evacuated to ~10^{-2} Pa and sealed quartz ampoules at

temperatures 50° higher than the melting temperatures of the synthesized compounds. The ampoules with the obtained melts were kept at these temperatures for 3-4 hours and then cooled in the switched off furnace to room temperature. We used high purity simple substances from the company Evochem Advanced Materials GMBH: copper granules (Cu-00029; 99.9999%), antimony granules (Sb-00002; 99.999%), tin pieces (Sn-00003; 99.9999%), selenium granules (Se-00002; 99.999. The individuality of all synthesized compounds was monitored by differential thermal analysis (DTA) and powder X-ray diffraction (PXRD) methods (%). About twenty Cu_3SbSe_4-$SnSe_2$ alloys were prepared by alloying the initial compounds under vacuum conditions. According to DTA data for cast non-homogenized alloys, it was shown that their crystallization from melts is completed at temperatures not lower than 660 K. Taking this into account, to achieve a state as close as possible to equilibrium, cast alloys obtained by rapid cooling of melts were annealed at 630 K within 700 hours.

The prepared samples of the studied system were investigated by DTA and PXRD methods. DTA was performed on a 404 F1 PEGASUS SYSTEM differential scanning calorimeter (NETZSCH). The heating rate was 10 K·min-1. The DTA measurement results were processed using the NETZSCH Proteus Software. The temperature measurement accuracy was within ±2°.

PXRD was carried out at room temperature on a BRUKER D8 ADVANCE diffractometer with CuKα1 radiation. The X-ray patterns were indexed using the Topas V3.0 Software Bruker.

Results and discussion.XRD analysis of the annealed samples showed that Cu_3SbSe_4-$SnSe_2$ alloys containing no more than 20 mol.% $SnSe_2$ are single-phase and have diffraction peaks identical to those for the pure Cu_3SbSe_4 compound with a slight shift to the right (Fig. 1).

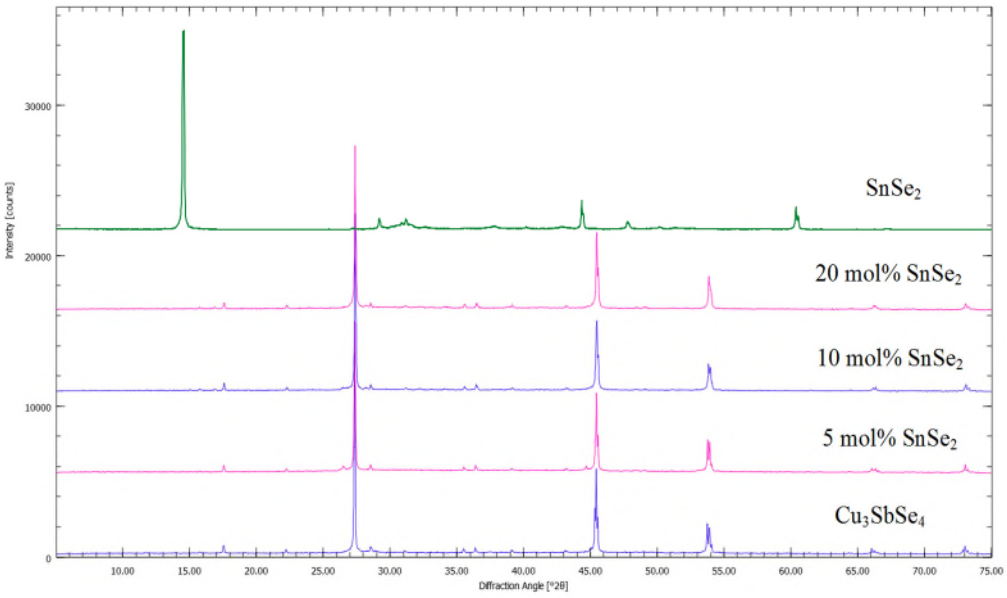

Fig.1. PXRD patterns for the Cu_3SbSe_4-$SnSe_2$ alloys

This indicates the formation of up to 20 mol% solid solution based on the Cu_3SbSe_4 compound. The PXRD patterns of alloys with concentration < 20 mol% $SnSe_2$ are indexed in tetragonal structure. The following lattice parameters were calculated by indexing these powder diffraction patterns:

Cu_3SbSe_4 a=5.6531 Å; c=11.2606 Å;
$(Cu_3SbSe_4)0.95\ (SnSe_2)0.05$ a=5.6509 Å; c=11.2505 Å;
$(Cu_3SbSe_4)0.9\ (SnSe_2)0.1$ a=5.6421 Å; c=11.251 Å;
$(Cu_3SbSe_4)0.8\ (SnSe_2)0.2$ a=5.6371 Å; c=11.2407 Å;

The formation up to 20 mol% solid solution area in the investigated system was confirmed also by DTA method. We could not interpret the DTA data for alloys with more than 20mol% $SnSe_2$.

Phase equilibrium in $SnSe_2$-rich composition is complicated. So, we determined the phase compositions of the alloys in the entire range of compositions of the investigated section by means of PXRD method. It was found that in the 20-57 mol% $SnSe_2$ compositions range alloys consist of a 4-phase mixture α+Cu_2SnSe_3+Sb_2Se_3+Se. The alloy with a composition of 60 mol% $SnSe_2$ is 3-phase: Cu_2SnSe_3+ +Sb_2Se_3+Se. Alloys containing more than 60 mol% $SnSe_2$ consist of a 4-phase mixture Cu_2SnSe_3+ +Sb_2Se_3+$SnSe_2$+Se. For example, Fig.2 shows a powder X-ray diffraction pattern of an alloy containing 80 mol% $SnSe_2$ with an indication of the phase composition.

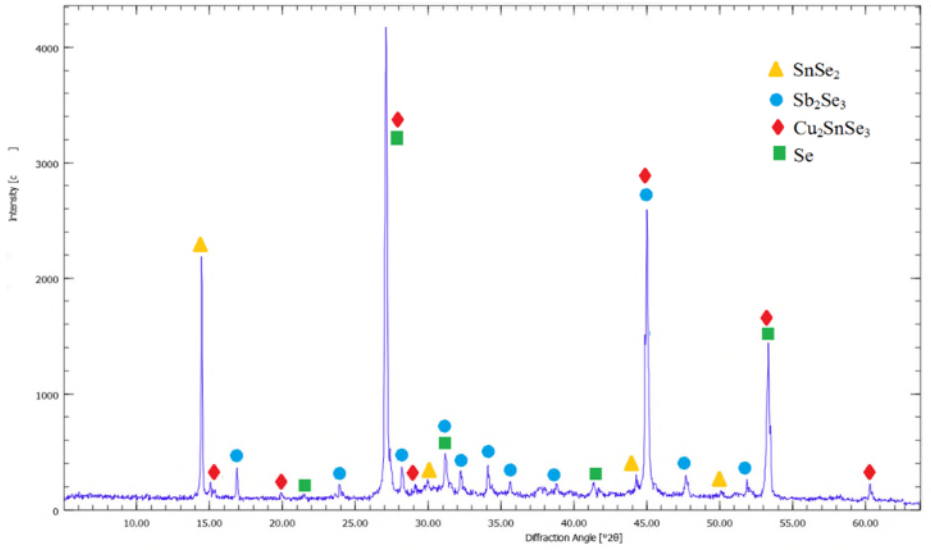

Fig.2. Powder diffraction pattern of the Cu_3SbSe_4-$SnSe_2$ alloy with a content of 80 mol% $SnSe_2$

Based on the data obtained, it can be concluded that the Cu_3SbSe_4-$SnSe_2$ section is located in 4-phase regions Cu_3SbSe_4+Cu_2SnSe_3+Sb_2Se_3+Se and Cu_2SnSe_3+Sb_2Se_3+$SnSe_2$+Se of the concentration tetrahedron Cu_2Se-$SnSe_2$-Sb_2Se_3-Se. These areas are delimited by a stable concentration triangle Cu_2SnSe_3-Sb_2Se_3-Se. The composition of the alloy located on the plane of this triangle corresponds to 60 mol% $SnSe_2$.

Note, that our study of the similar systems Cu_3SbX_4-$GeSe_2$ (X=S,Se) showed a similar phase equilibria view [22,23]. Thus, in these systems up to 15 mol% solid solution based on the starting ternary compound is observed.

So, the formation of abnormally large solid solution areas based on starting ternary compounds in the studied Cu_3SbX_4-$MeSe_2$ (Me= Ge, Sn; X=S, Se) systems (replacement of 15-20% of Sb^{5+} cations with Me^{4+} ions) can be explained by fact, that the crystallographic radius of these ions does not differ sharply from each, and other hand, the load balance during $Sb^{5+} \rightarrow Me^{4+}$ substitutions is ensured by the conversion of some Cu^{1+} ions to Cu^{2+}. This prevents the formation of additional vacancies in the cationic lower cage.

Conclusion

The character of phase equilibria in the Cu_3SbSe_4-$SnSe_2$ system has been established by DTA and PXRD methods. The formation in the system up to 20 mol% of solid solutions based on Cu_3SbSe_4 is shown. Phase equilibria in the $SnSe_2$-rich area are complex and alloys consist of various heterogeneous mixtures. The obtained solid solutions are interesting as potential environmentally friendly functional materials.

References

1. Hegazy H.H. Semiconducting chalcogenide Ge-Se-Sb-Cu as new prospective thermoelectric materials. // J. Results in Physics. – 2019. – Vol.14. – Pp.102-492.

2. Chalcogenides: Advances in Research and Applications. / Woodrow Phillips (Editor). Nova. – 2018. – P.111.

3. Babanly M.B., Mashadiyeva L.F., Babanly D.M., Imamaliyeva S.Z., Tagiyev D.B. and Yusibov Yu.A. Some Issues of Complex Investigation of the Phase Equilibria and Thermodynamic Properties of the Ternary Chalcogenid Systems by the EMF method // Russ. J. Inorg. Chem. – 2019. – Vol.64, №13. – P.1649-1671. doi:10.1134/S0036023619130035

4. Andrzej M., Krzysztof M., Paweł N., and Paweł R. Copper Chalcogenide–Copper Tetrahedrite Composites–A New Concept for Stable Thermoelectric Materials Based on the Chalcogenide System. // Materials. – 2021, 14. – P. 2635. https://doi.org/10.3390/ma14102635

5. Zhang X., Zhao L.D. Thermoelectric materials: Energy conversion between heat and electricity. // J. of Materiomics. – 2015. – Vol.1. – Pp.92-105.

6. Sanghoon X.L., Tengfei L.J., Zhang L.Y-H. Chalcogenide. From 3D to 2D and Beyond. – Elsevier. – 2019. – P.398.

7. Qiu P., Shi X., & Chen L. Cu-based thermoelectric materials. // Energy Storage Mater. – 2016. – Vol.3. – Pp.85-97. doi:10.1016/j.ensm.2016.01.009

8. Zeier W.G., Zevalkink A., Gibbs Z.M., Hautier G., Kanatzidis,M.G., Snyder G.J. Thinking Like a Chemist: Intuition in Thermoelectric Materials. // Angew.Chem., Int. Ed. – 2016, 55. – Pp.6826-6841.

9. Li D., Li. R., Qin X.Y., Zhang J., Song C.J., Wang L., Xin H.X. Co-precipitation synthesis of Sn and or S doped nanostructured Cu_3Sb_1-xSnxSe_4-yS_y with a high thermoelectric performance. // Cryst.Eng.Comm. – 2013. – V.15. – Pp.7166-7170.

10. Wei TR., Wang H., Gibbs Z.M. et al. Thermoelectric properties of Sn-doped p-type Cu_3SbSe_4: a compound with large effective mass and small band gap. // Mater Chem. A. – 2014. –2. – Pp.13527-13533.

11. Heo J., Laurita G., Muir S, et al. Enhanced thermoelectric performance of synthetic tetrahedrites. // Chem Mater. – 2014, 26. – Pp.2047-2051.

12. Dandan X., Bin Z., Aijuan Z., Yongjin C., Yanci Y., Hengquan Y., Guiwen W., Guoyu W. et. al. High thermoelectric performance of Cu_3SbSe_4 nanocrystals with Cu_2–xSe in situ inclusions synthesized by a microwave-assisted solvothermal method. // Nanoscale. – 2018, 10. – P.14546.

13. Ghanwat V.B., Mali S.S., Bagade C.S., Mane R.M., Hong C.K., Bhosale P.N. Thermoelectric Properties of Indium(III)-Doped Copper Antimony Selenide Thin Films Deposited Using a Microwave Assisted Technique. // Energy Technol. – 2016. – Vol.4. Pp.835-842.

14. Prem Kumar D.S., Chetty R., Femi O.E. et al. Thermoelectric properties of Bi doped tetrahedrite // J. Elec. Mater. – 2017, 46. – Pp.2616-2622.

15. Jeffrey D.C., Donald T.M. High thermoelectric figure of merit in the Cu_3SbSe_4-Cu_3SbS_4 solid solution. // Appl. Phys. Lett. – 2011, 98. – P.261911; https://doi.org/10.1063/1.360 5246 Eric J. Skouga).

16. Ravaji K., Ezzati R., Mohammadi A.H., Abbas S.A. Electric and Thermoelectric Properties of $Cu_{12}Sb_4S_{13}$ Tetrahedrite with Impurities. // Preprints. – 2019. – Pp. 2019080051.

17. Liu Y., García G., Ortega S., et al. Solution-based synthesis and processing of Sn- and Bi-doped Cu_3SbSe_4 nanocrystals, nanomaterials and ring-shaped thermoelectric generators. // J. Mater Chem. A. – 2016, 5. – Pp.2592-2602.

18. Lu X., Morelli D.T., Xia Y., et al. High performance thermoelectricity in earth-abundant compounds based on natural mineral tetrahedrites. // Adv Energy Mater. – 2013, 3. – Pp.342-348.

19. Pet L., Christophe C., Anne D., Janusz T., Jiří H. and Bertrand L. Thermoelectric properties of the tetrahedrite–tennantite solid solutions $Cu1_2Sb_4$–xAsxS_{13} and $Cu_{10}Co_2Sb_4$–yAsyS_{13} ($0 \leq x, y \leq 4$). // Phys. Chem. – 2019. – Vol.21. – Pp.4547-4555.

20. Li X.Y., Li D., Xin H.X., et al. Effects of bismuth doping on the thermoelectric properties of Cu_3SbSe_4 at moderate temperatures. // J. Alloys Compd. – 2013, 561. – Pp.105-108.

21. Ismayilova E.N., Baladzhayeva A.N., Mashadiyeva L.F. Phase Equilibria Along the Cu_3SbSe_4-$GeSe_2$ Section of the Cu-Ge-Sb-Se System. // New Materials, Compounds and Applications. – 2021. – Vol.5, №1. – Pp.52-58.

22. Баладжаева А.Н., Исмайлова Э.N., Шевельков А.В., Бахтиярлы И.Б., Машадиева Л.Ф. Фазовые равновесия по разрезу Cu_3SbS_4-GeS_2 системы Cu-Ge-Sb-S. / Межд.науч. конф. «Актуальные проблемы современных природных и экономических наук» 06-07 мая, Гянджа. – 2021. – С.12-16.

23. Ismayilova E.N., Shukurova G.M., Aliyeva E.R., Mashadieva L.F. Polythermal Section SnSe–$CuSbSe_2$ of Phase Diagram of the Cu_2Se–SnSe–Sb_2Se_3 System // Azerb. Chem. – 2018, № 4. – Pp.29-32.

24. Pfitzner A. Crystal Structure of Tricopper Tetraselenoantimonate (v), Cu_3SbSe_4 // Zeitsch. für Kristallog. // Crystal. Mater. – 1994, 209(8). – Pp.685-685.

25. Massalski T.B. & Okamoto H. Binary alloy phase diagrams-CD-ROM. // Mater.Park. – OH: ASM International. – 1996.

26. Palosz B. & Salje E. Lattice parameters and spontaneous strain in AX_2 polytypes: CdI_2, PbI_2, SnS_2 and $SnSe_2$. // Appl. Cryst. – 1989. – Vol.22. – Pp.622-623.

Xülasə

Ismayılova E.N.

Cu_3SbSe_4-$SnSe_2$ sistemində faza tarazlıqlarının rentgenoqrafik tədqiqi

Cu-Sn-Sb-Se sisteminin Cu_3SbSe_4-$SnSe_2$ kəsiyi üzrə faza tarazlıqları DTA və RFA metodları ilə tədqiq edilmişdir. Sistemdə Cu_3SbSe_4 əsasında Sb → Sn əvəzləməli bərk məhlulların (α-faza) əmələ gəldiyi aşkar edilmişdir. Bərk məhlulların homogenlik sahəsi 20 mol% -ə çatır. Sistemdə $SnSe_2$ ilə zəngin sahədə faza tarazlıqları mürəkkəbdir. Tədqiq olunan kəsiyin xəlitələrinin bütün qatılıq boyu faza tərkibləri RFA üsulu ilə müəyyən edilmişdir: α+Cu_2SnSe_3+Sb_2Se_3+Se (20-58 mol% $SnSe_2$); Cu_2SnSe_3+Sb_2Se_3+Se (60 mol% $SnSe_2$); Cu_2SnSe_3+Sb_2Se_3 + $SnSe_2$ + Se (60 mol% $SnSe_2$-dən çox).

Açar sözlər: mis əsaslı halkogenidlər, faza tarazlığı, sistem, mis-sitibium selenid, bərk məhlullar.

News of Azerbaijan Higher Technical
Educational Institutions
ISSN 1609-1620
Volume 23, № 5 (2021), 26-29
UDC 665.61

Development of method metal naphthenates production

Chemistry and chemical technology

Bayramova A.R.
Azerbaijan State Oil and Industry University,
E-mail: ayten_bayramova_91@mail.ru

One of the requirements of modern times is the involvement of heterogeneous compounds in oil, along with oil and gas hydrocarbons, to create a strong raw material base for the petrochemical industry. From the hydrogen compounds in oil, the most suitable are the oxygenated compounds of oil – the separation and purification of naphthenic acids from oil and the synthesis of practically useful compounds based on them. From this point of view, metal naphthenates of naphthenic acids – Fe, Cu, Ba, Co, Cr and other naphthenates have special properties. These salts of naphthenic acids can be used as oxidizing catalysts with high thermal stability, antistatic added to oils and fuels, anti-corrosion, detergents, additives added to paints and varnishes, as well as stimulants in the production of colored asphalts and petroleum-based substances used in road construction. Natural acids from oil are mainly 95-98% (mass) naphthenic acids, and the remaining substances are fatty, aromatic or condensed radical acids, phenols and resin-asphalt substances. Molecular fatty acids is a limitation of the scope of their mixtures.

Keywords: oil, naphthene, metal naphthenate, hydrocarbon, resin asphalt substances.

Introduction

The object of the research was alkaline wastes from the alkaline treatment of distillates processed at the atmospheric vacuum unit of the marine oil mixture from the oil refinery named after H.Aliyev.

According to the literature, petroleum naphthenic acids that have been used so far are small-molecule (containing up to C_{12} carbon atoms in the molecule) kerosene-gasoyl fractions.

Substances based on petroleum naphthenic acids are distinguished by special technical useful properties.

The naphthenic radical in the acid molecule gives special properties to its derivatives: the freezing point is reduced, thermooxidation and hydraulic stability are improved, the solubility is increased, the viscosity – temperature, mechanical, anti-corrosion, etc. properties are improved.

Statement of the problem

As it is known, in order to separate fuel and oil distillates from petroleum naphthenic acids at the H.Aliyev refinery, distillates are treated with an aqueous solution of sodium hydroxide and sodium salts of naphthenic acids are dissolved in aqueous solution and are called "alkaline waste" in the plant practice. These alkaline wastes are completely decomposed with mineral acids to obtain "crude" naphthenic acids or factory acids. Alkaline wastes usually contain large amounts of neutral hydrocarbons in the sodium salts of naphthenic acids.

Solution methods

Shake the alkaline waste sample vigorously by adding a few drops of methyl orange and 10% HCl acid until the sodium soap breaks down. After a few minutes, the red color of the aqueous solution in the separating funnel indicates the complete decomposition of the sodium soap.

To dissolve naphthenic acids and oil (organic part), add 35-40 ml of petroleum ether, boiling at 40-60 ° C, to the separating funnel and shake. After storage for half an hour, the lower water layer obtained in the funnel,s separated from the upper ether layer. To neutralize traces of mineral acid in the ether layer, wash it with a solution of sodium sulfate or common salt until a neutral reaction is obtained (methyl indicator). After each wash, the solution is stirred and stored for 10 minutes.

The organic matter in the petroleum ether is dried by means of dry sodium sulphate, filtered through a paper filter and transferred to a beaker of known weight, washed three times with fresh ether, separated on the filter and then added to the ether layer in the beaker.

Petroleum ether is placed on the water bath and then the glass is left for 5 minutes to completely expel the residue of ether, keep in a thermostat with a temperature of 105 ° C. The residue is cooled and weighed.

We used the following method to obtain metal naphthenates.

First, the alkaline salts of petroleum naphthenic acids (for example, Na, K) are obtained, then the aqueous solution of the alkaline salts is obtained by the interaction of metals with the aqueous solution of salts, metallic naphthenates:

$$RCOOH + NaOH \rightarrow RCOONa + H_2O$$

$$2RCOONa + MeCl_2 \rightarrow (RCOO)_2\,Me + 2NaCl,$$

here R – the radical of naphthenic, Me = Cu, Mn atoms.

To obtain naphthenates, NaOH is added to naphthenic acid and mixed vigorously. The resulting sodium solution has a white cloudy color, pH = 7 (LP-58). After evaporation of the solution, a yellowish-white plastic substance is released, which is also soluble in organic substances (kerosene, gasoline and benzene).

Similarly, potassium naphthenates were obtained. For example, for the production of (RCOO) 2Ni naphthenates, a certain amount of RCOONa solution was placed in the separating funnel, and an appropriate amount of NaCl2 (1 mg / ml Ni + 2) gasoline (solvent) was added to the separating funnel at the same time. After mixing (hemogenization) for 1 hour, we kept the mixture until it was completely stratified (1 day). The pH of the water phase and the amount of residual nickel are determined.

We determined the extraction percentage according to the following formula:

$$E = \frac{\alpha \cdot 100}{\alpha + (\upsilon_{wat.}/\upsilon_{sur.})},$$

here α – distribution coefficient; $\upsilon_{wat.}$, $\upsilon_{sur.}$ – is the volume of water and organic matter in water and organic phase, respectively (ml).

As a result, the yield of 2Ni-nickel naphthenate (RCOO) was 30.2%, similarly, Mn, Cu, Zn, Co, etc. Naphthenates of metals were obtained and their extraction rate was between 30-32%.

Al, Cr, Fe, Ni, Co, Mo salts of naphthenic acids separated from the kerosene fraction and vacuum-cleaned from neutral hydrocarbons were obtained by the above method. Hydroxides, chlorides and aqueous solutions of sulfate salts of these metals were used in the production of these salts and a number of their properties were studied.

Results and discussion

Studies show that some of these naphthenates are soluble in water and the rest are precipitated from the solution. Some properties of the obtained metal naphthenates are given in Table.

Table. Properties of low molecular weight naphthenates

Naphthenates	Output, % (mass.)	Color	Soluble in organic matter						
			Gasoline	Kerosene	CCl_4	C_6H_6	Ether	Oil	Alcohol
$(RCOO)_2Fe$	56,2	White	+	-	+	-	-	+	-
$(RCOO)_2Ni$	50,3	Light green	+	+	+	+	+	+	-
$(RCOO)_2MO$	48,5	Brown	+	+	+	+	+	+	+
$(RCOO)_2CO$	45,6	Blue	+	+	+	+	-	+	-
$(RCOO)_2Zn$	52,3	Yellow	+	+	+	+	-	+	-
$(RCOO)_2Cd$	47,9	White	+	+	+	+	+	+	-
$(RCOO)_2Mn$	95,7	Indigo	+	+		+	+	+	+
$(RCOO)_2Cu$	47,7	Blue	+	+	+	+	+	+	-
$(RCOO)_2Cr$	45,8	Blue	+	+	+	+	+	+	+

Naphthenates of heavy metals, as a rule, in the form of plastic, colored masses, have a low softening temperature. (RCOO) 2Ni is a solid compact mass of light green color, (RCOO) 2Mn is a glassy mass that is insoluble in water, (RCOO) 2CU is a blue soft mass. They are well extracted with kerosene, benzene and gasoline (at pH = 8.5).

Aluminum and chromophthenates are also obtained by the exchange reactions of naphthenic acids with sodium salts of water-soluble salts of Al and Cr.

Conclusion

The following method has been developed for the production of naphthenates based on petroleum naphthenic acids.

Alkaline salts of naphthenic acids are first obtained (K, Na), and then metal naphthenates are synthesized by the exchange reaction with the salts of any metal.

The results of the research showed that during the production of metal naphthenates, almost all of them take on the color of cations, some of them are soluble in water and various solvents. The discovery of these properties creates new opportunities for their use as additives in fuels and oils, mixing naphthenates with marble chips and other grabbers, and their application in road construction.

References

1. Burge H. Bioaerosols: prevalence and health effects in the indoor environment. // Journ. of Allergy and Clinical Immunol. – 1990. – Vol.86. – Pp.687-701.

2. De Hoog G.S., Guarro J., Gene J., Figueras M.J. Atlas of clinical fungi. // Utrecht: CBS. – Spain: Reus, 2000. – 1126 p.

3. Aliyev F., Badalov A., Huseynov E., Aliyev F. // Ecology. – Baku: Science, 2012. – P.828.

4. Fung F., Hughson W.B. Health Beffects of indoor fungal bioaerosol exposure. // Appl. Occup. Environ. Hyg. – 2003. – Vol.18, №7. – Pp.535-544.

5. Compton O.C Plant tissue monitoring for fluorides. // Hortseince. – 1970. – Vol.45, № 4. – Pp.244-246.

6. Collas F. Production of isopropanol, butanol and ethanol by metabolic engineered Clostridia. // Agro Paris Tech. – Paris, 2012.

Xülasə
Bayramova A.R.
Metal naftenatların alınması üsulunun işlənib hazırlanması

Müasir dövrün tələblərindən biri də neft -qaz karbohidrogenləri ilə birlikdə neftə daxil olan heterogen birləşmələrin neft -kimya sənayesi üçün güclü bir xammal bazası yaratmaqdır. Neftdəki hidrogen birləşmələrindən ən uyğun olanı oksigenli yağ birləşmələridir - naften turşularının neftdən ayrılması və təmizlənməsi və onların əsasında praktiki olaraq faydalı birləşmələrin sintezi. Bu baxımdan naftenik turşuların metal naftenatları – Fe, Cu, Ba, Co, Cr və digər naftenatlar müəyyən xüsusiyyətlərə malikdir. Bu naftenik turşuların duzları yüksək istilik sabitliyinə malik oksidləşdirici katalizatorlar, yağlara və yanacaqlara antistatik əlavə, korroziyaya qarşı, yuyucu vasitələr, boyalara və laklara əlavə maddələr, həmçinin rəngli asfalt və neft əsaslı istehsalda stimulantlar kimi istifadə edilə bilər (yol tikintisində istifadə olunan maddələr). Neftdən alınan təbii turşular, əsasən, 95-98% (kütləvi) naften turşuları, qalan maddələr isə yağlı, aromatik və ya qatılaşdırılmış radikal turşuları, fenollar və qatran-asfalt maddələrdir. Molekulyar yağ turşuları qarışıqların əhatə dairəsini məhdudlaşdırır.

Açar sözlər: neft, naften, metal naftenat, karbohidrogen, rezin asfalt birləşmələri.

News of Azerbaijan Higher Technical
Educational Institutions
ISSN 1609-1620
Volume 23, № 5 (2021), 30-35
UDC 666.945

Influence of copper-smelting slag on the grindability of amorphous electrothermophosphorus slag

Mechanics and machine-building

Gaziev U.A., Mukhamedbaev A.A., Abdazov D.R., Saydullaev A.B.
Tashkent Institute of Architecture and Civil-Engineering
E-mail: devon@taqi.uz

Annually, as a result of human activity, many tons of waste of various man-made genesis are formed. Some of them are copper-smelting and electrothermophosphorus slag. Various options and ways of utilization of these wastes are well known. Among them, the most promising direction is the production of slag-alkali binders which are an alternative substitute for the traditional Portland cement. One of the labor- and energy-intensive processes of this technology is a separate and combined grinding of aluminosilicate components in a ball mill. This article presents the results of studies of joint grinding of copper-smelting and electrothermophosphorus slag in a ball mill.

Keywords: copper-smelting slag, electrothermophosphorus slag, grindability, ball mill, grinding fineness, slag-alkali binders.

Introduction

Pyrometallurgical production of non-ferrous metals is characterized by formation of a large amount of production wastes, the main of which are slags [1]. Thus, 2-4 tons of smelting, converter and refining slag are generated in copper-smelters (CS) when producing a ton of copper. The integrated use of technogenic wastes, which include slags, creates prerequisites for saving natural resources and strengthening the mineral resource base of non-ferrous metals.

Metallurgical slags are industrial byproducts [2], most of which are recycled by stacking or dumping. Colossal quantities of industrial smelting slag or waste dumps occupy large areas of land and cause great damage to the environment. The best way to solve this problem is to turn metallurgical slags into new value-added materials [3], which will also bring enormous economic benefits to society.

At the pyrometallurgical method of obtaining copper in the smelting furnaces of the CSP of JSC "Almalyk mining and smelting plant" a large amount of dumped slag is formed. Slags of the copper plant: reflection smelting slag - 5,439,503 tons; oxygen flaring slag - 1,836,117 tons; slag in liquid bath smelting - 724,380 tons; a total of 8,000,000 tons [4].

CS slag can be used as a component of the raw mix of portland cement clinker or as a mineral additive in the production of general construction cements [5].

The possibility of using granulated slag, a waste product of CS production, as an auxiliary component of mineral additive in cement grinding for general construction purposes has been considered [6]. The composition, properties and grindability of CS slag, its effect on grinding time, granulometric composition and physical and mechanical properties of cements have been studied.

In addition to the production of cement, slag from CS production can be used as a raw material component in obtaining slag-alkali binders. Many studies have established [7,8] that slag-alkali binders are not only inferior, but in some characteristics are superior to cement binders. Distinctive features of this technology is the absence of high-temperature firing, the use of solid wastes of metallurgy

and chemical industries as raw materials, the binder mixing with alkaline aqueous solutions, the absence of CO_2 emissions into the atmosphere, etc. [9,10].

The authors of paper [11] obtained alkali-activated cement material. In the study the raw components copper slag, sodium silicate solution, sodium hydroxide, water and sand were completely mixed in the ratio 1000:330:56:135:3000. It was found that in this case the compressive strength of the cement material at 28 days of age reached 34.12 MPa.

It is well known that alkali activated binders are greatly influenced by the type and chemical composition of the alkaline activator [12,13], the conditions of sample hardening [14], the dispersibility of the aluminosilicate (slag) component [15,16], etc.

It is well known that the highest physical and mechanical properties of slag-alkali binders are achieved when using granulated slag as an aluminosilicate component. One of such is electrothermophosphorus (ETP) slag [17-19]. ETP slag is a waste product of yellow phosphorus production by electrothermal sublimation, obtained by rapid cooling of silicate melt formed in electric furnaces during the melting of charge mixture of phosphate ore, quartzite and coke. The production of 1 ton of phosphorus yields 10-14 tons of fire-liquid slag.

The main labor- and energy-consuming technological process in this technology is separate or joint grinding of aluminosilicate components [20-24]. In this aspect, the study of slag milling is relevant and not fully studied. Previously, we investigated the milling processes of ETP itself and with the addition of various surfactants and mineral components [25-29].

In this case, the most important parameters of grinding fineness are the specific surface area, the residue on the sieve number No. 008, the average grain diameter, bulk density, etc. [15,16, 24, 30-33].

Statement of the problem

These studies were aimed at studying the effect of CS slag on the grindability of ETP slag in a ball mill.

Solution methods

CS slag and ETP slag were used in the study. CS slag was used by the plant of the CSP of JSC "Almalyk mining and smelting plant". CS slag is dumped and not granulated. The color of CS slag is black. Chemical composition of CS slag by weight (%): SiO_2 – 38,9; Al_2O_3 – 11,32; Fe_2O_3 – 35,6; CaO – 9,8; MgO – 1,5; SO_3 – 0,74; CuO – 0,49; firing loss – 0,7. The phase composition is mainly represented by glass phase, fayalite, and magnetite.

ETP slag was used in the Republic of Kazakhstan. The structure of ETP slag is represented by a vitreous phase (90-98 %) of metasilicate composition having a microhomogeneous structure. The crystalline phase is pseudovolastonite. Chemical composition of ETP slags by weight (%): SiO_2 – 34,0-45,0; Al_2O_3 – 1,07-3,29; CaO – 44,7-50,0; MgO – 0,91-4,38; F – up to 3; P_2O_5 – up to 2,5.

Photographs of CS and ETP slag are shown in Fig. 1.

a) *b)*

Fig.1. Photographs of slags: a) copper-smelting slag; b) electrothermophosphorus slag

Grain composition of ETP slag is given in Table1 [25].

Table 1. Grain composition of ETP slag

No. of sieves	Partial residue, %	Total residue, %	Size modulus
2,5	7	7	2,93
1,25	24	31	
0,63	38	69	
0,315	23	92	
0,14	7	99	
bottom	1		

Grinding was carried out in a laboratory ball mill MBL-1. Steel balls and cones were used as grinding bodies. The duration of milling was 45-75 minutes. The mass of the grinding bodies and the material to be ground in all cases was constant.

The specific surface area, residue on the sieve No. 008, bulk density and average grain diameter were determined as parameters of fineness. The specific surface and the average diameter of grains were determined on the device PSX-11A. The operating principle of the device is based on the determination of gas permeability by the Carman-Kozeny method. The measurement method consists in determining the time of passage of a fixed volume of air through a layer of the sample. Bulk density was determined using a standard liter vessel and a funnel.

Results of the study and their discussion. Initially, the ETP slag itself was milled in a ball mill. The results showed (Fig.2) that to achieve a specific surface area of ≈3000 cm^2/g between 65-70 minutes.

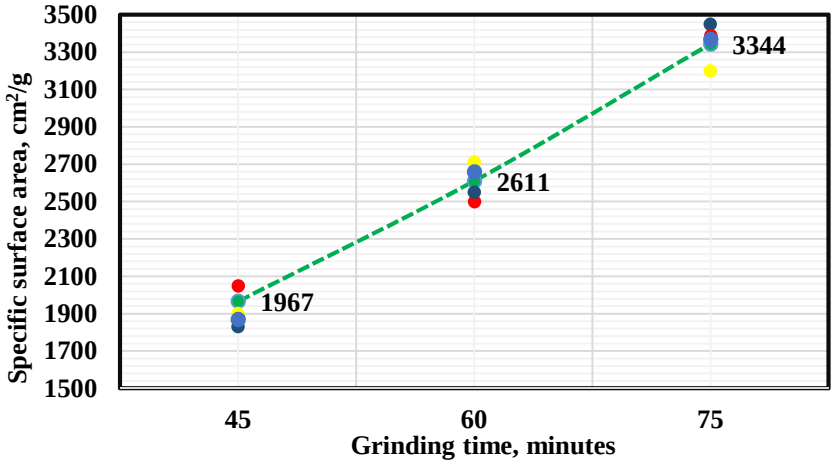

Fig.2. Values of specific surface of ETP slag as a function of grinding time

Table 2. Characteristics of grindability

Component ratio, %		Specific surface area, cm^2/g	Residue on the sieve №008, %	Average grain diameter, μm	Bulk density, g/cm^3	Intergrain hollowness
CS slag	ETP slag					
15	85	3597	3,0	6,0	1,02	0,47
30	70	4668	4,2	4,6	1,08	0,53
45	55	3912	6,4	5,5	1,10	0,47
60	40	4210	4,2	5,1	1,13	0,48

As shown by the results of co-milling grindability (Table 2), that in each case milling has a peculiar character. The maximum values of specific surface area were reached in composition №2. The average grain diameter of the milled powders varied between 4,6-6,0 microns, depending on the ratio of the components (Fig.3). The values of bulk density in the unconsolidated state remained in the range of 1,02-1,13 g/cm^3. Intergrain hollowness was in the region of 0,47-0,53. The amount of residue on the sieve No. 008 was 3,0-6,4 %.

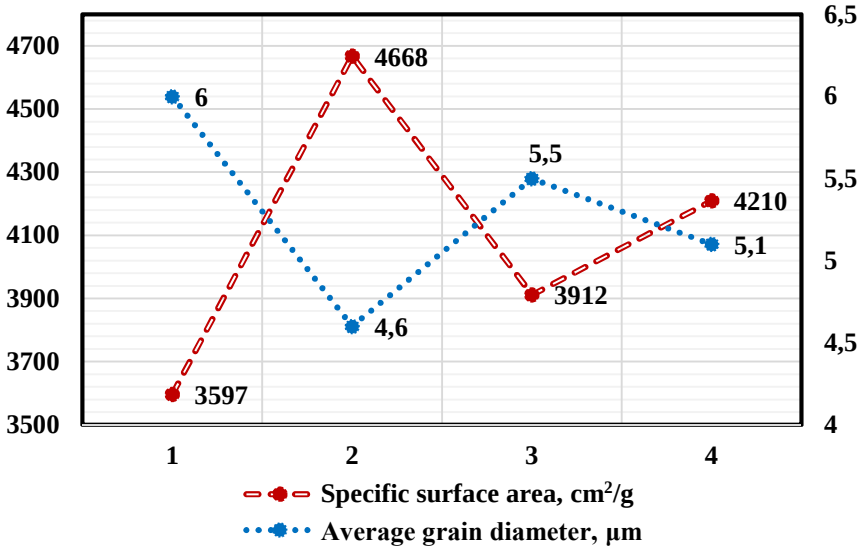

Fig. 3. Specific surface area and average grain diameter values:
1 – 15% CS+85% ETP; 2 – 30% CS+70% ETP;
3 – 45% CS+55% ETP; 4 – 60% CS+40% ETP.

Conclusion

As a result of studies it was found that depending on the ratio of CS and ETP slag, the kinetics of grindability in a ball mill changes. For more accurate assessment of fineness in each case requires not only determination of values of specific surface and residue on the sieve No. 008, but also the average grain diameter and bulk density of a finely ground product.

References

1. Харченко Е.М., Ульева Г.А., Егорова Т.Г., Рахимбеков С.С. Переработка шлаков медеплавильного производства. // Международный журнал прикладных и фундаментальных исследований. – 2015, № 7-1. – С.30-33.

2. Zhang T., Zhi S., Li T., Zhou Z., Li M., Ha J., Li W., Zhang D., Guo L., Wu Z. Alkali Activation of Copper and Nickel Slag Composite Cementitious Materials. // Materials. – 2020, 13. – P.1155. https://doi.org/10.3390/ma13051155

3. Liu K., Zhang Z., Sun J. Advances in Understanding the Alkali-Activated Metallurgical Slag. // Advances in Civil Engineering. – 2021. https://doi.org/10.1155/2021/8795588

4. Хакимов К.Ж., Хасанов А.С., Каюмов О.А., Шукуров А.Ю., Соатов Б.Ш. Изучение химического вещественного состава шлаков медеплавильного производства, кеков, клинкеров и других отходов металлургических производств. // Universum электрон. научн. журн. – 2021, 2(83). https://7universum.com/ru/tech/archive/item/11313

5. Классен В.К. Борисов И.Н., Мануйлов В.Е. Техногенные материалы в производстве цемента. – Белгород: БГТУ, 2008. – 126 с.

6. Капустин Ф.Л., Афанасьева М.А. Использование медеплавильного шлака в производстве цементов общестроительного назначения. // Alitinform. – 2013, №3 (30). – С.52-58. https://alitinform.ru/articlenoce/ispolzovanie-medeplavilnogo-shlaka-v-proizvodstve-cementov-obshhestroitelnogo-naznacheniya

7. Palomo A., Krivenko P., Garcia-Lodeiro I., Kavalerova E., Maltseva O., Fernandez-Jimenez A. A review on alkaline activation: new analytical perspectives. // Materiales de Construccion. – 2014. – V.64. http://dx.doi.org/10.3989/mc.2014.00314

8. Yao Ding, Jian-Guo Dai, Cai-Jun Shi. Mechanical properties of alkali-activated concrete: A state of the art review. // Construction and Building Materials. – 2016. – Vol.127. – Pp.68-79. https://doi.org/10.1016/j.conbuildmat.2016.09.121

9. F. Pacheco-Torgal et al. Alkali-activated binders. / A review. Part 2. About materials and binders manufacture. Review. Construction and Building Materials. – 2008, 22. – Pp.1315-1322.

10. Rajesh D.V.S.P., Narender Reddy A., Venkata Tilak U., Raghavendra M. Performance of alkali activated slag with various alkali activators. // International Journal of Innovative Research in Science, Engineering and Technology. – 2013. – Vol. 2, Issue 2. – Pp.378-386.

11. Singh J., Singh S.P. Development of Alkali-activated Cementitious Material using Copper Slag. // Constr. Build. Mater. – 2019. 211:73–79. doi: 10.1016/j.conbuildmat.2019.03.233.

12. Gong Y.F., Fang Y.H., Yan Y.R., Chen L.Q. Investigation on alkali activated recycled cement mortar powder cementitious material. // Materials Research Innovations. – 2014. – Vol.18, № 2. – Pp.784-787.

13. Xin L., Jin-yu X., Weimin L., Erlei B. Effect of alkali-activator types on the dynamic compressive deformation behavior of geopolymer concrete. // Materials Letters. – 2014., Vol.124. – Pp.310-312.

14. Ben Haha M., Saout G.Le. Winnefeld and Lothenbach. Influence of activator type on hydration kinetics, hydrate assemblage and microstructural development of alkali activated blast-furnace slags. / Cement and Concrete Research. – 2011. – Vol.41, №3. – Pp.301-310.

15. Камилов Х., Тулаганов А., Хасанова М., Мухамедбаев А., Камилов Ш. Механоактивация безобжиговых щелочных вяжущих. / Монография: под ред. д.т.н., проф. Тулаганова А. – Т.: Fan va texnologiya, 2016. – 176 с.

16. Мухамедбаев Аг.А. Механоактивация алюмосиликатного компонента безобжигового щелочного вяжущего. // Журнал «Сухие строительные смеси». – М., 2017, №5. – С.35-37.

17. Грызлов В.С., Федорчук Н.М., Бейсекова Т.И. Электротермофосфорные шлаки как основа вяжущих композитов. // Строительные материалы. – 2014, №10. – С.66-69. https://cyberleninka.ru/article/n/elektrotermofosfornye-shlaki-kak-osnova-vyazhuschih-kompozitov/viewer

18. Сарсенбаев Б.К., Момышев Т.А., Искаков Т.У., Сарсенбаев Н.Б., Аубакирова Т.С. Производство шлакощелочных вяжущих и бетонов на их основе. // Строительные материалы. – 2012, №12. – С.56-57. https://cyberleninka.ru/article/n/proizvodstvo-shlakoschelochnyh-vyazhuschih-i-betonov-na-ih-osnove/viewer

19. ГОСТ 3476-2019. Шлаки доменные и электротермофосфорные гранулированные для производства. – М.: Стандартинформ, 2019.

20. Артамонова А.В., Воронин К.М. Шлакощелочные вяжущие на основе доменных гранулированных шлаков центробежно-ударного измельчения / Цемент и его применение. – 2011. – С.108-113. https://uralomega.ru/files/shlakowelochnye_vyazhuwie na osnove_domennyh_ granulirovannyh_shlakov_centrobezhno-udarnogo_izmel_cheniya.pdf

21. Suman Saha, Rajasekaran C. Enhancement of properties of fly ash based geopolymer paste by incorporating ground granulated blast furnace slag. // Construction and Building Materials. – 2017. – Vol.146. – Pp.615-620. https://doi.org/10.1016/j.conbuildmat.2017.04.139

22. Petrakis E., Karmali V., Bartzas G., Komnitsas K. Grinding Kinetics of Slag and Effect of Final Particle Size on the Compressive Strength of Alkali Activated Materials. // Minerals. – 2019, 9. – P.714. DOI: 10.3390/min9110714

23. Акопян А.Ф. Исследование механических и технологических свойств шлакощелочных вяжущих, полученных с использованием добавки комплексного действия. // Известия вузов. Северо-Кавказский регион. – 2010, №4. – С.65-68. https://cyberleninka.ru/article/n/issledovanie-mehanicheskih-i-tehnologicheskih-svoystv-shlakoschelochnyh-vyazhuschih-poluchennyh-s-ispolzovaniem-dobavki/viewer

24. Хасанова М.К., Камилов Х.Х., Мухамедбаев Аг.А. Особенности процесса помола гранулированного шлака в шаровой мельнице. // Сухие строительные смеси. – 2016, №1. – С.25-27.

25. Мухамедбаев Аг.А., Камилов Х.Х., Хасанова М.К., Тулаганов А.А. Особенности процесса помола электротермофосфорного шлака и его смесей. // Химия и химическая технология. – 2016, № 1. – С.58-61.

26. Мухамедбаев Аг.А., Камилов Х.Х., Тулаганов А.А. Модифицированные шлакощелочные вяжущие. // Научно-технический журнал ФерПИ. – Фергана, 2019, № 3. – С.74-78.

27. Мухамедбаев Аг.А. Механоактивированные многокомпонентные щелочные вяжущие и пенобетоны на их основе. / Дисс. на соис. уч. степ. докт. филос. (PhD) по техн. наукам. – Ташкент, 2019. – 120 с.

28. Kamilov Kh.Kh., Mukhamedbaev A.A., Abdazov D.A. Influence of Fly Ash on The Grindability of Electrothermophosphorus Slag. // International Journal of Scientific Research in Science, Engineering and Technology. – 2021. – Vol.8, Issue 3. – Pp.536-544. https://ijsrset.com /paper/7187.pdf

29. Adilkhojaev A.I., Kadirov I.A. On the mechanoactivation of metallurgical waste. European Journal of Research Development and Sustainability. – 2021. – Vol.2, №5. – Pp.60-67. https://scholarzest.com/index.php/ejrds/article/view/784/662

30. Мухамедбаев Аг.А., Тулаганов А.А., Камилов Х.Х., Мухамедбаев А.А., Яичников Я.М. Способ определения тонкости помола. / Патент IAP 06008 UZ. Заяв.: 11.06.2014; опуб.: 31.10.2019. Бюл. № 10. – Ташкент.

31. Мухамедбаев Аг.А. Исследование влияния времени механоактивации на свойства многокомпонентного вяжущего. // Вестник Пермского национального исследовательского политехнического университета. Строительство и архитектура. – Пермь, 2018. – Т.9, № 3. – С.121-129. DOI: 10.15593/2224-9826/2018.3.12

32. Mukhamedbaev Ag.A. Slag-alkaline foam concrete based on granulated electrothermophosphorus slag. // Journal «European science review». – Viena, 2018. – Vol.1., № 9-10. – Pp.192-195. https://cyberleninka.ru/article/n/slag-alkaline-foam-concrete-based-on-granulated-electrothermophosphor-slag

Xülasə

Qaziyev U.A., Muhamedbəyov A.A., Abdazov D.R., Saydullayev A.B.

Misəritmə şlakların amorf elektrotermofosforlu şlakların pardaqlanmasına təsiri

Hər il insan fəaliyyəti nəticəsində müxtəlif texnogen genezisli bir çox ton tullantı əmələ gəlir. Bunlardan biri misəritmə və elektrotermofosfor şlaklarıdır. Bu tullantıların utilizasiyasının müxtəlif variantları və üsulları məlumdur. Bunların arasında ən perspektivli istiqamət ənənəvi Portland sementinin alternativi olan şlak-qələvi bağlayıcıların istehsalıdır. Bu texnologiyanın zəhmət və enerji tələb edən proseslərindən biri də alüminosilikat komponentlərinin kürəli dəyirmanda ayrı və birgə üyüdülməsidir. Məqalədə kürəli dəyirmanda misəritmə və elektrotermofosforlu şlaklarının birgə üyüdülməsi ilə bağlı aparılan tədqiqatların nəticələri təqdim edilmişdir.

Açar sözlər: misəritmə şlakları, elektrotermofosforlu şlaklar, pardaqlama, kürəli dəyirman, üyüdülmə incəliyi, şlak-qələvi bağlayıcılar.

News of Azerbaijan Higher Technical
Educational İnstitutions
ISSN 1609-1620
Volume 23, № 5 (2021), 36-38
UDC 621.791

Methods providing sealing in mechanical engineering

Mechanics and machine-building

Ragimova M.S., Gafarov F.M., Namazova G.I.
Azerbaijan State Oil and Industry University
E-mail: Rahimova_mahluqa@mail.ru

In modern mechanical engineering, oilfield machinery is characterized by a wide range of units, equipment and tools. The efficient operation of machinery and equipment must be ensured by the high level of maintenance provided to them in a timely manner. Before starting to assembly the flange joints, it is necessary to check the tightness of the flange surfaces. Leakage occurs for a number of reasons: including maintenance, improper installation and repair. The sealing surfaces of the flange should be thoroughly cleaned, and no crumbs or dents should be allowed on their surface. Such defects should be eliminated by polishing. Radial scratches are very dangerous. When assembling the flange joints, care must be taken to ensure that its sealing surfaces are strictly parallel. However, once the surfaces are parallel, it is necessary to tighten the nuts on the pins. In this case, the parallelism of the sealing surfaces is controlled by means of a shup tool. One of the main factors determining its tightness is that it is cold and kept in working condition. From the operating condition of the flange joint during cold drawing; the pins must be pulled with a certain force to repel the force created by the internal pressure of the working medium. When designing various construction working in liquid and gaseous environments can be provided in two ways:
– by creating a non-detachable connection elements by soldering, welding;
– by riveting, or by sealing detachable joints using various means.

Keywords: gasket, sealing, sealant, detachable and non-detachable connections, leak proofers.

Introduction

The creation of non-detachable joints by welding, riveting and soldering is often not possible due to the structural or operational characteristics of the parts (for example, disconnection of knots during the exploitation process).

Non-sealant compounds may include compounds between metal-metal, plastic and rubber parts.

Statement of the problem

In mechanical engineering, metal-metal compounds are mainly used in non-sealant joints. In this case, the seal is provided by the contact of the micro-profiles of the sealing surfaces. The degree of seal depends on the quality and properties of the contact surfaces, but it is also directly related to the processing methods of the contact surfaces. At the same time, the actual contact between the metal surfaces of the touching parts does not exceed 25-50% during the most perfect treatment (machining).

Solution methods

To determine the level of a given sealing, the modeling of the surface profile is solved as follows.

First, the parameters of the surface layer of the meeting parts are determined. These parameters help to ensure the required sealing, and then the reatment modes are determined to help achieve certain surface parameters [3].

This method makes it possible to ensure the required level of sealing at an early stage of product design.

Gasket elements are used in the automotive industry to ensure the sealing of immovable detachable joints. The main purpose of the gasket elements is to fill the roughness of the sealing surfaces due to elastic-plastic deformations.

The sealant is made of both metallic and non-metallic materials. There is no generally accepted classification of sealing elements. This is due to the fact that the seals have different shapes. They are often classified according to the principle of influence and their belonging to definite area.

Sealants made of metal are used in heavy-duty conditions: in the cylinder head and cylinder block head, etc. At the same time, these products are exposed to high pressures, as well as temperature differences and aggressive environments. Aluminum (AD and others), steel (12X18H10T, SS304, SS316, 05KP, etc.), bronze (L63, etc.), copper and other materials are used to make metal gaskets.

Non-metallic sealants include rubber, paronite, fluoro-plastics, silicone and anaerobes (liquid sealants). At the same time, leather, paper, cardboard, fiber, and other materials are used as sealing materials. Sealants must be able to withstand deformation, ensure the recovery of deformation of flange joints in the case of a change in operating mode, have low cost and simple construction.

Polymeric materials are widely used in modern automotive industry and the number of polymers used is growing.

Gradually, the quality and performance characteristics of new materials used increase.

The materials are resistant to aggressive environments (gasoline, oil, chemicals, etc.) and used for a long time in harsh conditions [2].

The limits of operating temperature variation are widened and for some materials they exsud 300^0C.

This creates a great potential for the use of polymer gaskets in the creation and repair of machines and competes with traditional gaskets made of rubber, paronite and metal.

The purpose of the use of polymer gaskets is to place the first qualitatively stable part of the flange surfaces.

Most joints found in modern technology are sealed with the help of sealing elements. Metal sealants are used at high temperatures and pressures. However, most joints use non-metallic sealants. At the same time, the use of so-called "liquid sealants" is growing. This type of sealants successfully replaces sealants made of traditional materials (rubber, paronite, etc.). This is explained by the high performance characteristics of "liquid gasket". Such " gasket" are resistant to various liquids.

The gradual displacement of traditional gasket materials by polymer "liquid gaskets" is due to many reasons. Such high-tech materials are chemically resistant to aggressive fuels and oils. They provide high structural strength for various joints. Rubber-like silicone sealants are conveniently placed on sloping and vertical surfaces. Many metal joints are assembled with the help of anaerobic sealants. This, firstly, provides additional rigidity of the joint, and secondly, sizes of the knot in question do not change and the sealing of the joint is increased.

At the same time, such contaminants have less noise than metal-metal joints [1].

The presence of a sound-absorbing layer between the friction surfaces reduces the specific noise of the unit. Despite the advantages of using new materials, their application is associated with certain difficulties.

Sometimes it is not possible to use sealants in the process of repairing machine units. The quality of manual sealing is reduced, because it is very difficult always to keep the gap between the sealing surface and the part held.

Conclusion

Based on the above, it can be said that the optimal gasket in production is carried out without human intervention. This is because the lack of a worker's qualification level leads to a violation of the sealing technology, and the sealing joint becomes unusable for further operation.

References

1. Kondakov L.A. and others. Sealing and sealing equipment. // Handbook. – M.: Machine building. – 1994. – 445 p.

2. New elastomeric material. New Elastomermaterial from Hitze and Kraftstoff in Motorraum. // MTZ. – 2008, 69, №2. - P.115.

3. Calculation of acoustic characteristics. Rechnergestütztes Verfahren zur akustischen Optimize rung van Dichtungen. // MTZ. – 2005, 66, №5. – Pp.386-393.

Xülasə

Rəhimova M.S., Qafarov F.M., Namazova G.İ.

Maşınqayırmada kipliyin təmin olunması üsulları

Müasir maşınqayırmada neft-mədən texnikası çoxçeşidli aqreqatlarla, avadanlıqlarla və alətlərlə xarakterizə olunur. Maşın və avadanlıqların səmərəli istismarı, onlara göstərilən yüksək səviyyəli texniki xidmət vaxtında ehtiyat hissələrlə təmin olunmalıdır. Fləns birləşmələrinin yığımına başlamamışdan əvvəl araqatını və fləns səthlərinin kipliliyinə baxmaq lazımdır. Kipliyin pozulması bir sıra səbəblər üzündən baş verir: istismar, düzgün yerinə yetirilməyən quraşdırma və təmir daxildir. Flənsin kiplik səthlərini əsaslı surətdə təmizləməli, onların səthində qırıntı və tilişkələrə yol verilməməlidir. Bu cür qüsurları pardaxlama ilə aradan götürmək lazımdır. Radial sıyrıntıların olması çox təhlükəlidir. Fləns birləşmələrinin yığımı zamanı onun kipləyici səthlərinin ciddi surətdə paralel olmasına diqqət yetirmək lazımdır. Ancaq səthlərin paralel olmasını əldə etdikdən sonra sancaqlarda olan qaykaların bərabər çəkib bağlanmasını həyata keçirmək lazımdır. Bu zaman kipləyici səthlərin paralel olmasına şup aləti vasitəsilə nəzarət edilir. Kipliyini müəyyən edən əsas amillərdən biri onun soyuq halda çəkilməsi və işçi şəraitdə saxlanmasıdır. Soyuq çəkilmə zamanı fləns birləşməsinin işləmə şərtindən; işçi mühitin daxili təzyiqindən yaranan qüvvəni dəf etmək üçün sancaqlar müəyyən qüvvə ilə çəkilməlidir. Su və qaz mühitlərində işləyən müxtəlif konstruksiyaların layihələndirilməsi zamanı kipliyin iki üsulla təmin olunması nəzərdə tutulur:

– söküləbilməyən birləşmələr tərəfindən, yəni qaynaq, pərçim, lehimləmə və s.;

– söküləbilən birləşmələrin qarışıq yerlərinin kipliyinin müxtəlif üsullarla təmin olunması.

Açar sözlər: araqatı, kiplik, kipləyici, söküləbilən və söküləbilməyən birləşmələr, kiplik dərəcəsi.

News of Azerbaijan Higher Technical
Educational Institutions
ISSN 1609-1620
Volume 23, № 5 (2021), 39-46
UDC 631-317.7; 621-319

Tracking system for tension stabilization small section wires

Energetics and energetic machine-building

Abdullaev Ya.R., Kerimzadeh G.S., Mammadova G.V.
Azerbaijan State Oil and Industry University
E-mail: gulschen98@mail.ru

In order to calculate and study the characteristics of a tracking system with levitation screens, a mathematical model was formed on the basis of analytical expressions for currents, equivalent inductance, voltages, temperature differences, lifting electromagnetic force and dimensionless values of the magnetic system. Analytical expressions for the dimensions and parameters of the tracking system were obtained from the solutions of the mathematical model, which made it possible to investigate the relationship between the main parameters. The graphs of generalized functional dependencies have been obtained, with the help of which it is possible to determine the optimal values of the working air gap of the dimensions of the magnetic circuit and the levitation screen.

Keywords: wire tension stabilization, tracking system, mathematical model, equivalent inductance, number of turns, excitation winding, levitation screen, generalized functional dependencies.

Introduction. Tension of tape or long materials is one of the main technological parameters that determine the quality characteristics of products obtained by the winding method in electrical, textile, paper and other industries [1-5]. When carrying out winding work in the process of manufacturing coils, one of the conditions for high-quality winding and increasing the winding speed is to maintain a constant tension of the wire during the winding process [6]. In some devices, for example, in superconducting magnets, windings made from a winding wire with a diameter of less than 0.06-0.08 mm are used. For such devices, it is often necessary to provide a certain value of the active resistance of the winding. With small diameters of the winding wire, the tension of the wire during the winding process has a significant effect on the value of this resistance. In addition, when winding on rectangular frames, there are sharp changes in the tension of the wire during the transition of the wound wire from the edge to the edge of the rectangular frame. This can lead to wire breakage and requires a special device that would ensure the stabilization of the wire tension during operation. As this device, you can use a wire tension stabilizer [4], which works on the principle of a tracking system with levitation screens, which ensures high accuracy of wire tension control. The absence of friction between the elements of the tracking system with levitation screens (LS) and the unambiguous relationship between the output and input signals are undoubtedly the advantage of the tension device under consideration over the known ones.

The servo system under consideration (Fig.1*a*) consists of a master and receiver transducers (ЗП and ППП). Each transducer consists of a vertically located magnetic circuit 1 with a fixed winding excitation (EW) 2 and levitation screen (LS) 3. Excitation windings 2 ЗП and ППП are connected in series with each other and powered from a voltage source, with industrial frequency $\omega = 314\ s - 1$.

The dimensions of the ЗП and ППП are the same, the magnetic cores are made of sheet metal electrical steel, and LS - from aluminum in the form of a rectangular frame (Fig.1*b*).

Statement of the problem

To date, the calculation and optimization of the electromagnetic parameters of the tracking system with LS are absent, although the theory and calculation of magnetic systems with LS are based on a number of works, including works [5 - 8]. In this work, the thickness of the working air gap and the main dimensions of the LS and the magnetic circuit are determined. As is known [6], at a supply voltage frequency of 50 Hz the depth of penetration of an electromagnetic wave into a LS made of aluminum is about 14 mm. Therefore, the maximum value of the working air gap must be determined from these conditions. In addition, in the calculations, it is necessary to take into account the condition of the uniformity of the magnetic field in the working air gap $m_a = b/a = 1 \div 6$ and $m_c = b/c = 1 \div 6$. However, due to the scattering of the magnetic flux from the edges of the magnetic conductor rods, there is an additional magnetic conductivity, which, if not taken into account, leads to large errors in the calculations. In the calculations, we take the following assumptions: the current and voltage of the excitation winding are sinusoidal, the magnetic resistances of the steel sections are negligible compared to the magnetic resistances of the air sections.

Solution methods

Taking into account the above noted features and assumptions, we compose a mathematical model that is formed from:

- expressions of the EW and LE currents:

$$I_1 = \frac{k_u(0{,}5U_1)}{\omega L_1} \tag{1}$$

$$I_2 = b_2 I_1 \frac{W_1}{W_2} \tag{2}$$

- expressions of the equivalent inductance of the magnetic system:

$$L_1 = \lambda W_1^2 = \lambda(x_p + h_0)W_1^2 \tag{3}$$

- expressions of the condition of levitation:

$$F_Э = 0{,}5(I_1 W_1)^2 \lambda = P_T \tag{4}$$

- expressions on the terminals of the excitation winding (EW):

$$U_1 = A_1(W_1 \cdot S_c) \tag{5}$$

- expressions for the cross-sectional area of the middle rod of the magnetic conductor, where the EW is located:

$$S_c = 2ab = 2c^2 \frac{m_c^2}{m_a} \tag{6}$$

- expressions for the temperature difference between the EW and LE:

-

$$\tau_1 = \frac{P_1 + P_2}{k_T S_{T1}};\ \tau_2 = \frac{P_2}{k_T S_{T2}}. \tag{7}$$

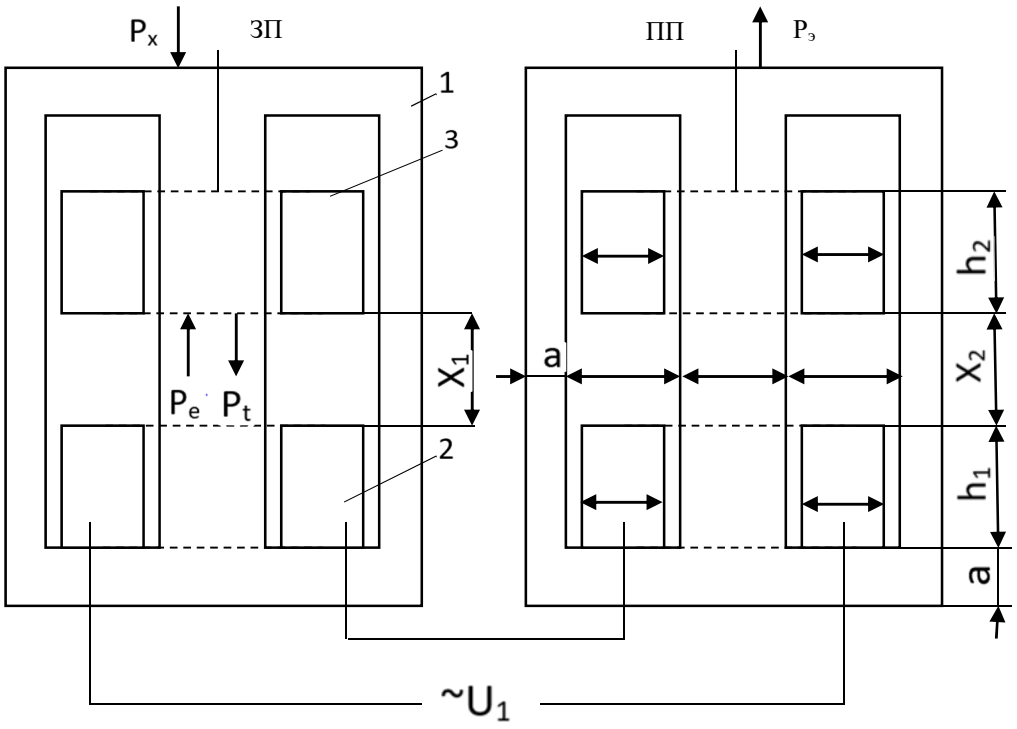

a

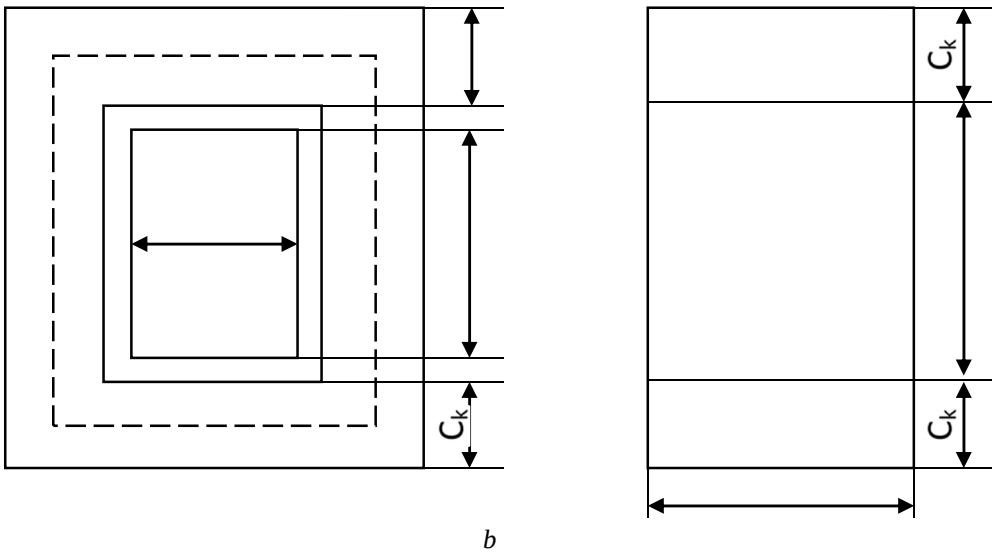

b

Fig. 1 Schematic diagrams of LSTS (*a*) and solid LS made of aluminum (*b*)

Here some designations are generally accepted [5,6,7], and other parameters are defined as:

$$\lambda = 2\mu_0 m_c \sigma_v; \quad \sigma_v = 1 + 2.92 \lg(1 + \frac{\pi}{m_a}) \tag{8}$$

$$A_1 = \frac{4\omega B_M}{k_u \sqrt{2}}; \quad m_a = \frac{b}{a}; \quad m_c = \frac{b}{c} \tag{9}$$

$$S_{T1} = h_1(l_1 + 4c); \quad S_{T2} = 2l_2 c_2 (1 + n_{e2}); \quad n_{e2} = \frac{h_2}{c_2} \tag{10}$$

$$l_1 = n_{01} \cdot c_1; \quad l_2 = 2c_2 k_0; \quad n_{01} \approx 1{,}05 \div 1{,}1 \tag{11}$$

$$P_1 = (I_1 W_1) \cdot \rho_1 j_1 l_1; \; P_2 = (I_2 W_2) \cdot \rho_2 j_2 l_2; \; I_2 W_2 = b_2 I_1 W_1 \tag{12}$$

The specific electrical resistances of the magnetic circuit of EW and LE made of aluminum are determined from the expression:

$$\rho_1 = 1{,}72 \cdot 10^{-8}(1{,}063 + \alpha_m \cdot \tau_1);\ \rho_2 = 2{,}78 \cdot 10^{-8}(1{,}0645 + \alpha_a \cdot \tau_2) \tag{13}$$

Determination of the main parameters. In the absence of an external force ($P_x = 0$), the inductances of the EW ЗП and ПП are equal and through the working stroke x_p of the levitation screen are determined according to (3):

$$L_1 = L_2 = \lambda W_1^2 (x_p + h_0), \tag{14}$$

where W – is the number of turns of the EW; λ – specific magnetic conductivity of the working air gap; $h_0 = h_1/3$ is the equivalent height of the EW. The specific magnetic conductivity of the working air gap, taking into account the magnetic flux of scattering, is determined from (9). Table 1 shows the values of the specific magnetic conductivity λ and the scattering coefficient σ_v. Inductance through the known parameters of the EW is determined by the formula

$$L_1 = \frac{k_u U_1}{2\omega I_1} \tag{15}$$

From (3) and (15) we obtain the identity:

$$\frac{x_p + h_0}{U_1} = \frac{k_u}{2\omega\lambda I_1 W_1^2} \tag{16}$$

The right side of expression (15) is a constant value, since I = const. Therefore, the value of the fraction with a change in voltage U_1 remains constant, with an increase in voltage U_1, the working stroke x_p increases, or vice versa. This feature of the servo system is an important property of the master transducer. From expression (5), we determine the number of turns of the EW as

$$W_1 = \frac{U_1}{A_1 \cdot S_c} \tag{17}$$

The inductance of the EW, taking into account (14) and (9), is written in the following form:

$$L_1 = 2\mu_0 m_c \sigma_v (x_p + h_0) W_1^2 \tag{18}$$

Then, according to (15) and (18), for the number of turns of the EW we obtain:

$$W_1^2 = \frac{m_1}{m_2 I_1 m_c \sigma_v \sqrt{2}}, \tag{19}$$

where indicated

$$m_1 = \frac{k_u U_1}{2\omega};\ m_2 = \mu_0 (x_p + h_0) \tag{20}$$

The obtained expressions explicitly show the relationship between the number of turns W_1 and the known values of the parameters U_1, ω, x_p, h_0 and I_1. It follows from (20) that taking into account the scattering coefficient $\sigma_в$ and dimensionless quantities $m_a = b/a$ and $m_c = b/c$ in the calculations is necessary to increase the calculation accuracy. Substituting (6) into (17), we obtain an expression for the functional dependence W_1 (m_1, m_a, B_m, s):

$$W_1 = \frac{m_{1u} m_a \sqrt{2}}{B_M c^2 m_2^2 2} = \frac{m_1 m_a}{B_M c^2 m_c^2 \sqrt{2}} \tag{21}$$

or

$$W_1^2 = \left[\frac{m_1 m_a}{B_m c^2 m_2^2 \sqrt{2}}\right]^2 \tag{22}$$

According to (18) and (22), we obtain the identity:

$$\frac{m_1}{m_2 I_1 m_c \sigma_a \sqrt{2}} = \left[\frac{m_1 m_a}{B_M c^2 m_c^2 \sqrt{2}}\right]^2 \tag{23}$$

From here, we determine the functional dependence of the thickness of the working air gap on the current I_1, the coefficients m_a and m_c:

$$c = k_m \sqrt[4]{I_1 \sqrt[4]{\frac{m_a^2}{m_c^3}\left[1 + 2.92\lg(1+\frac{\pi}{m_a})\right]}}, \quad (24)$$

where k_m – is determined through the specified values of the parameters in the design task:

$$k_m = \sqrt[4]{\frac{m_1 m_2}{B_m^2\sqrt{2}}} \quad (25)$$

After determining the thickness of the working gap c, the dimensions of the magnetic circuit a and b, the area S_c and the number of turns are calculated:

$$b = m_c c;\ a = \frac{b}{m_a};\ S_c = 2ab \quad (26)$$

$$W_1 = \frac{0{,}5U_1 k_u \sqrt{2}}{\omega B_M S_c} = \frac{m_1\sqrt{2}}{B_m S_c} \quad (27)$$

Table 1. The values of the specific magnetic conductivity of the working air gap $\lambda\cdot10^{-6}$ Hn /m and the scattering coefficient of the magnetic circuit σ_B

m_c \ m_a	2	3	4	5	6	$\sigma_в$ / λ	$\lambda_0\cdot10^{-6}$	Note
2	1,598	1,454	1,367	1,309	1,267	$\sigma_в$	5,024	$\Lambda=\lambda_0+\lambda_b$
	8,030	7,305	6,870	6,576	6,365	Λ		
3	1,399	1,303	1,245	1,206	1,178	$\sigma_в$	7,536	$\lambda_0=2\mu_0 m_c$
	10,543	9,817	9,382	9,090	8,877	Λ		
4	1,299	1,227	1,227	1,155	1,133	$\sigma_в$	10,048	$\lambda_b=2\mu_0\beta$
	13,055	12,329	12,329	11,600	11,388	Λ		
5	1,239	1,182	1,182	1,124	1,107	$\sigma_в$	12,56	$\beta=2\lg(1+\pi/m_a)$
	15,566	14,841	14,841	14,112	13,901	Λ		
6	1,2	1,151	1,151	1,103	1,089	$\sigma_в$	15,072	$\sigma_v=\lambda / \lambda_0$
	18,078	17,353	16,917	16,624	16,413	λ		

Study of the relationship between parameters. For this purpose, we will consider a tracking system that has the following design specifications: voltage at the EW terminals U_1 = 220V, current frequency f = 50 Hz, current value in EW I_1 = 1.5A. The height of the EW h_1 = 30 mm, the height of the LE h_2 = 21 mm, the working stroke x_p = 40 mm. We define:

$$m_1 = \frac{k_u U_1}{2\omega} = \frac{0{,}9\cdot 220}{2\cdot 314} = 315{,}286\cdot10^{-3}$$

$$m_2 = \mu_0(x_p + h_0) = 1{,}256\cdot10^{-6}(40+10+7)\cdot10^{-3} = 71{,}592\cdot10^{-9}$$

$$m_1 \cdot m_2 = 315{,}286\cdot10^{-3}\cdot 71{,}592\cdot10^{-9}$$

$$\sqrt[4]{\frac{m_1 m_2}{B_m^2\sqrt{2}}} = \sqrt[4]{\frac{22{,}5719}{1{,}4^2\sqrt{2}}}\cdot10^{-6} = 9{,}499\cdot10^{-3} \quad (28)$$

According to (24) and (28), we finally obtain the calculated expression for the functional dependence with (I_1, m_a, m_c):

$$c = 9{,}499\cdot10^{-3}\sqrt[4]{I_1}\cdot\sqrt[4]{\frac{m_a^2}{m_c^3}}\cdot\left[1{,}292\lg\left(1+\frac{\pi}{m_a}\right)\right] \quad (29)$$

For a given value of the current I_1 = 1.5A, Table 2 shows the calculated values of the thickness c. The calculation was made using the EXCELL program. In accordance with the calculated values of size c in Fig.2. the graphs of dependence c (m_a; m_c) are presented. At the same time, taking into account the condition $c_2 \geq 14$ mm (or with ≤15 mm) from Table 2, we select the values with and the corresponding values of the coefficients of the graph m_a, and m_c. For example, we choose c = 14.347 mm and we find m_a = 4; m_c = 2. In this case, c_2 = 13.347 mm.

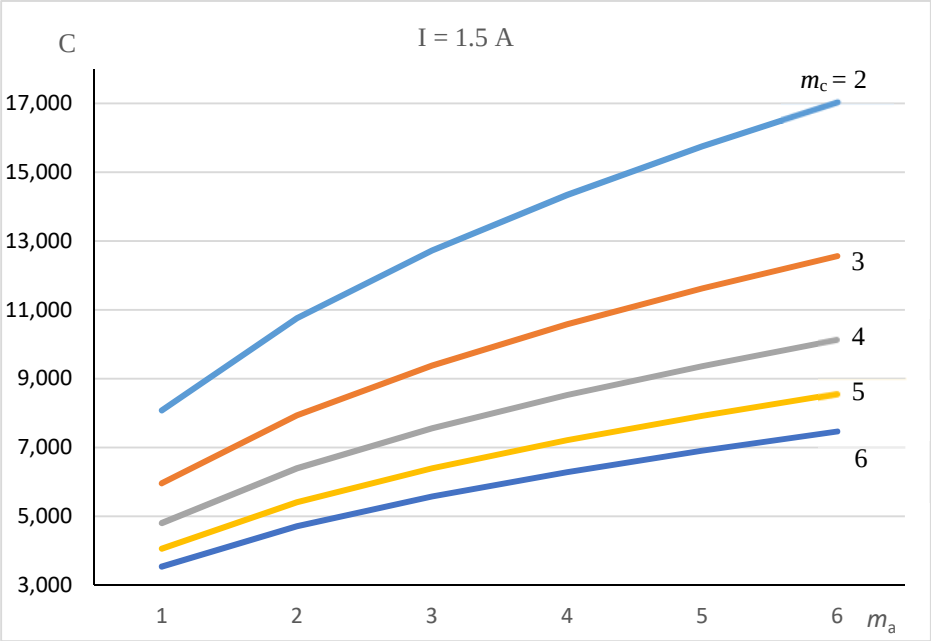

Fig. 2. Dependency plots c (m_a; m_c)

Table 2. Dimensions c in millimeters

m_c \ m_a	1	2	3	4	5	6
1	13.600467	18.099786	21.400335	24.129150	26.511384	28.656013
2	8.086886	10.762197	12.724716	14.347278	15.763763	17.038967
3	5. 966407	7. 940219	9. 388142	10.585249	11.630315	12.571145
4	4. 808491	6. 399241	7. 566161	8. 530943	9. 373190	10.131431
5	4. 067488	5. 413099	6. 400193	7. 216299	7. 928753	8. 570147
6	3. 547647	4. 721283	5. 582222	6. 294027	6. 915426	7. 474847

To analyze the relationship between the parameters based on Table 2, consider the following calculation options.

1. m_a = const; m_c = var; c = 14,347 мм; m_a = 4; m_c = 2.

We count $b = m_c \cdot c = 2 \cdot 14{,}347 = 28{,}694$ мм; $a = b/m_a = 28{,}694/4 = 7{,}173$ мм;

$S_c = 2ab = 411{,}672 \cdot 10^{-6}$ м^2; $W_1 = \dfrac{m_1\sqrt{2}}{B_M S_c} = \dfrac{315{,}286 \cdot 10^{-3}}{1{,}4 \cdot 411{,}672 \cdot 10^{-6}} = 547$.

2. m_a = const; m_c = var; c = 10,585 мм; m_a = 4; m_c = 3.

We count: $b = m_c \cdot c = 3 \cdot 10{,}585 = 31{,}755$ мм; $a = b/m_a = 31{,}755/4 = 7{,}938$мм;

$S_c = 2ab = 504{,}19 \cdot 10^{-6}$ м^2; $W_1 = \dfrac{m_1\sqrt{2}}{B_M S_c} = 631{,}166$.

3. m_c = const; m_a = var; c = 15,764 мм; m_a = 5; m_c = 2.

We count: b = $m_c \cdot c$ =31,528 мм; $a = b/m_a$ = 6,305 мм; $S_c = 2ab$ =397,605·10^{-6} м^2; $W_1 = \dfrac{m_1\sqrt{2}}{B_M S_c}$.

4. m_c = const; m_a = var; c =17,039 мм; m_a = 6; m_c = 2.

We count: $b = m_c \cdot c = 34{,}078$ мм; $a = b/m_a = 5{,}67$ мм; $S_c = 2ab = 387{,}103 \cdot 10^{-6}$ м^2; $W_1 = \dfrac{m_1\sqrt{2}}{B_M S_c} = 822{,}736$.

Analysis of the above calculations shows that there are a number of relationships between the parameters, which can be represented through generalized functional dependencies Π_1 (m_c), Π_2 (m_c),

Π_3 (m_a) and Π_4 (m_a). They are shown in Fig.3 and correspond for the cases m_a = const with m_c = const with m_a = var. The named dependencies are indicated by the following parameters:

$$\Pi_1 (m_c) – a; b; S_c; W_1 \text{ и } \Pi_2(m_c)\cdot c$$
$$\Pi_3(m_c) – b; c; W_1; \ \Pi_4(m_a) – a; S_c.$$

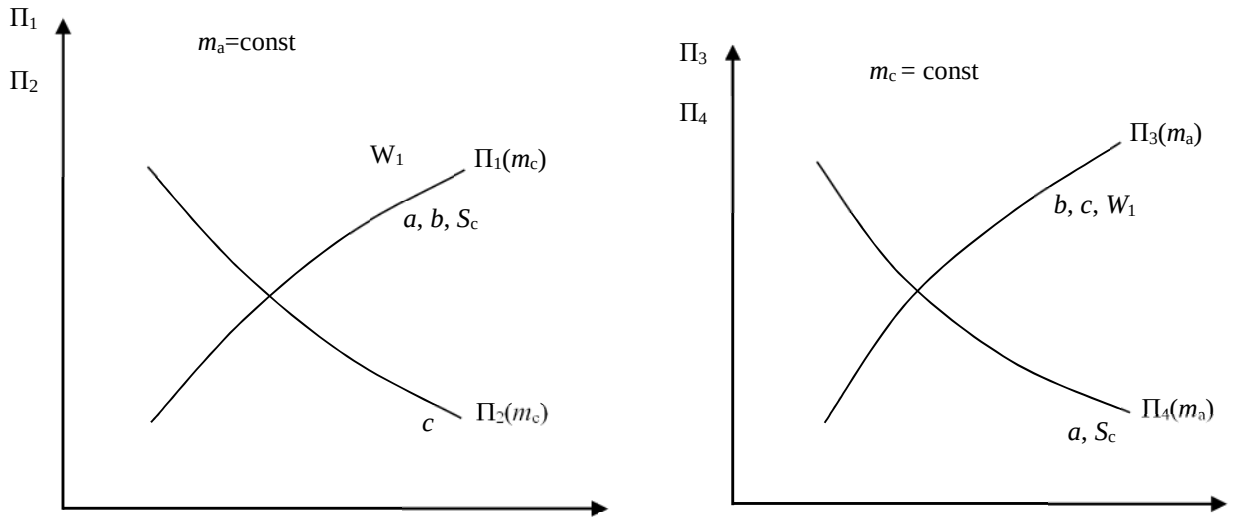

Fig.3. Generalized functional dependencies Π_1 (m_c), Π_2 (m_c),Π_3 (m_a) and Π_4 (m_a) for the cases a = const with m_c = const with m_a = var

Under the condition m_a = const, an increase in the coefficient m_c leads to an increase in the sizes a and b, the number of turns W_1 and the area S_c. In this case, the thickness c decreases. Taking these regularities into account, it is not difficult to choose the optimal values of sizes and parameters. However, under the condition m_c = const, an increase in m_a leads to an increase in the sizes c and b, the number of turns W_1. But in this case, the size a and the cross section S_c decrease.

Conclusion

1. A mathematical model of the tracking system has been compiled, which is the main unit of the device for accurate stabilization of the tension of wires of small cross-sections during the process of winding onto the frame.

2. Analytical expressions are obtained from the solutions of the mathematical model for the dimensions and parameters of the tracking system, which made it possible to study the relationship between the main parameters and characteristics.

3. The graphs of generalized functional dependencies have been obtained, with the help of which it is possible to determine the optimal values of the working air gap of the dimensions of the magnetic circuit and the levitation screen.

References

1. Bondarev N.I., Lisovskaya G.G., Mikhailov V.V., Martyshenko O.P. Electromechanical systems for monitoring and controlling the tension of tape materials. // Energy. – 1980. – 96 p.

2. Hoffman D. Measurement technique and quality assurance. / Reference. – M.: Energoatomizdat. – 1983. – P.472.

3. Measurements in industry. / Directory. ed. Ed. P. Profos translated from it. – M.: Metallurgy, 1980. – 648 p.

4. Abdullaev Ya.R., Alekseev A.V. Device for tension stabilization of long material. / A.S. №933553. B.I. – 1982, №21.

5. Abdullaev Ya.R. Theory and application of multifunctional linear induction suspensions. - Baku: Military publishing house, 1996. – P.297.

6. Abdullaev Ya.R. Theory of magnetic systems with electromagnetic screens / Monograph. – M.: Main edition of physical and mathematical literature. ed. "Science", 2000. - P.288.

7. Abdullaev Ya.R., Kerimzadeh O.O. Determination of the size of the DC magnetic system taking into account the principle of proportionality. – M.: Electricity, 2010, №3. – Pp.46-55.

8. Abdullaev Ya.R., Kerimzadeh G.S., Mamedova G.V., Pirieva N.M. Design of electrical devices with induction levitation elements. // Electrical engineering. – 2015, №4.

Xülasə

Abdullayev Y.R., Kərimzadə G.S., Məmmədova G.V.

Kiçik tellərin gərginliyini sabitləşdirmək üçün izləyici sistem

Levitasiya ekranlı izləyici sistemin xarakteristikalarının hesabı və tədqiqi məqsədilə cərəyanlar, ekvivalent induktivlik, gərginliklər, temperatur düşgüləri, maqnit sistemin qaldırıcı elektromaqnit qüvvəsi və ölçüsüz kəmiyyətlərin analitik ifadələri əsasında riyazi model formalaşdırılmışdır. Riyazi modelin həllindən izləyici sistemin ölçüləri və parametrləri üçün analitik ifadələr alınmış və əsas parametrlər arasındakı qarşılıqlı əlaqələrin tədqiqinə imkan yaradılmışdır. Ümumiləşdirilmiş funksional asılılıqların qrafikləri alınmışdır ki, onların vasitəsilə maqnitkeçirici və levitasiya ekranın ölçülərinin işçi hava aralığının optimal qiymətlərini təyin etmək olar.

Açar sözlər: tellərin gərginliyinin sabitləşməsi, izləyici sistem, riyazi model, ekvivalent induktivlik, sarğılar sayı, təsirlənmə dolağı, levitasiya ekranı, ümumiləşdirilmiş funksional asılılıqlar.

News of Azerbaijan Higher Technical
Educational Institutions
ISSN 1609-1620
Volume 23, № 5 (2021), 47-50
UDC 621.314.017

The impact of technological processing on the magnetic properties of electrical steel and the loss of transformers

Energetics and energetic machine-building

Veliyeva T.D.
Azerbaijan State Oil and Industry University
E-mail: veliyeva.tarana@mail.ru

Studies conducted for cold-rolled transformer steel exposed to impacts have shown deterioration of its magnetic properties. The deterioration in the quality of steel in turn leads to an increase in losses in the transformer. The work offers ways to reduce losses in the transformer, which can be taken into account in the process of production of transformers.

Keywords: steel, loss, transformer, loss factor, payload factor, magnetic flow, magnetic field induction.

Introduction. It is known that the process of making magnetic systems consists of several separate stages, for which special specific processing methods and special technological equipment are used [I].

One of the most important indicators of the quality of the magnetic wire is the loss increase efficiencies (L), which show how many times the loss in the real magnetic wire has increased compared to the losses in the original steel from which the active part of the magnetic wire is made, with the same calculated induction

$$L = \frac{P_{\text{magnetic wire}}}{P_{\text{original steel}}},$$

where $P_{\text{magnetic wire}}$ – is the magnetic unit losses in the magnetic wire; $P_{\text{original steel}}$ – unit losses in the original steel.

Losses in the magnetic system of the transformer are inevitable and are caused by the nature of steel magnetization. The increase in overall losses in steel magnet wire can be caused by mechanical effects on it during processing. The increase in losses in the magnetic wire is determined to a large extent by the technology of its production. The low level of the technology of the magneto-wire's gui can cause a significant increase in losses in the finished magnetic wire.

From the experience of domestic and foreign transformer-building from the news that for the same structures of magnetwires the factor of increase of losses has the following values:

- K=1,2-1.3 – for plants with advanced technology;
- K =1.6-2.0 – for low-tech plants.

Statement of the problem

The technological process is largely predetermined by the design of the magnetic wire, especially the type of blanks and the way they are articulated.

The main type of structures of magnetic wire are flat flaps, spatial plate-tape docking and spatial tape continuous. The technological processes of these structures have both common and their own specific benefits [2].

The existing technology of magnetic wire does not allow the full use of electromagnetic properties, which originally possesses electrical steel. After mechanical processing (cutting, stamping, removal of burrs, storage and transportation of plates, etc.) the deterioration of magnetic permeability of steel is detected, and in the collected magnetic wire - an increase in losses in steel and idleness.

The use of roll steel, mechanization and automation of the cutting process significantly improved performance, but retained all mechanical operations that reduce the magnetic properties of the source material. What's more, the inevitable either lines of longitudinal (or transverse) cutting bends and tension of the roll tape also add tension to the plates.

Solution methods

Minor deterioration of the magnetic properties of steel on each of this process processing lead in the finished magnetic wire to feel the increase in the initial level of losses, which sometimes it is impossible to revolt even repeated icing.

Cutting the plates leads to their deformation and creates a residual zone on the buckle (sticker) along the edge of the cut. The width of the sticker area 2-4 mm. The influence of the sticker is especially noticeable at the plates of small width up to 100-120 mm. Sticker increases the loss in steel by 3-5%.

In the process of cutting on automatic lines, steel is also bent (on drums) and the tension needed to move the tape. At the same time in the plates there are additional mechanical losses of tension. If the total impact of stresses from bending and stretching exceeds (8-9)*10 Pascal, then magnetic properties deteriorate and losses in steel increase.

In the process of cutting and stamping, burrs are formed as the tool fades and the gap between the cutting edges on the plates is blurred. The most common way to remove burrs is to roll them on special sunset swaths. The plates of steel are passed between the swaths and "squeezed" by them all over the surface. At the same time, the entire surface of the plates receives residual mechanical stresses – a rivet that increases the loss in steel and the current idling.

When removing burrs (rolling along the direction of rolling) on sheets of cold-rolled electrical steel there is an increase in unit losses by 6-7% and magnetizing current by 60% at nominal induction, and when rolled at an angle of 55 degrees to the direction of rolling, the loss of steel remains at the baseline.

When harvesting, transporting, storing plates and assembling a magnetic wire, transformer steel is subjected to multiple mechanical impacts associated with shock loads.

Studies have shown that magnetic properties deteriorate in cold-rolled transformer steel that has been hit. Moreover, the higher the quality of steel, the greater its sensitivity to shock loads. Due to the lack of special shelving and stands for assembling tape wires on the line of cutting and stamping plates, plates are often dumped into a pack; after the trans porting to the assembly site, they are again dropped from a height of 0.3-0.5 m, with shock loads, increased losses and magnetizing current in steel. It has been established that a single drop of a package of ten sheets of 0.35 mm thick from a height of 0.5 m increases losses by 5%, and magnetizing current by 10% [3].

Analysis of the results. As you know, the efficiency of the transformer is very high. But as a result of repeated energy transformation, energy losses on the way from station to consumer are 4-5%. Therefore, reducing energy losses remains one of the main tasks of transformer production. The gross knowledge of the causes of losses and ways to reduce them is absolutely necessary for the successful development and competent execution of any production operations during assembly. Consider first the losses in steel. It is very important to know how steel losses depend on the quality of performance in the production operations [4].

As a result of the research and analysis, the following methods are recommended to reduce the decline in steel:

1. Reducing the magnitude of the magnetic flow of F_0. This is the most unprofitable way, as to create the same electric forces would need to increase the number of turns in windings, that is, to spend more copper or aluminum wires.

2. It is more expedient, without reducing the magnetic flow, to use such electro-technical steel, which would have high resistance (to reduce the flow of vortex flows) and lowered losses on hysteresis, such as the roll of electric steel marks 3406, 3407, 3408.

3. Making a magnetic transformer system from thin insulated plates 0.30-0.28 mm thick instead of 0.35 mm, which drastically reduces the loss from vortex currents. Electrical steel 0.30 mm thick has a loss of 7% lower than the same 0.35 mm thick mark.

4.Making a magnetic transformer system with oblique layers by us. In magnetic systems collected from cold-rolled textured steel, the rectangular shape of the plates and the straight joints of the rod and yarn plates contribute to the appearance of increased losses and decreases of the magnetic permeability of steel in the area of the pairing of rod and yoke. Therefore, these magnet systems should be collected with oblique joints of plates in all or part of the joints of rods and yokes. The reduction in idling losses is up to 12%.

5. Making a magnetic system transformer from the same brand of steel. The magnetic system of the transformer should be made of the same brand and thickness of electrical steel. This will contribute to the resulting idling losses. However, transformer plants on different brands 3404, 3405. 3406, 3407, 3408 electrical steel with different thicknesses of 0.35, 0.30 mm, and in the process of making plates of the process of mixing them. In such cases, it becomes almost impossible to manufacture a magnetic system transformer from one brand of steel, which accordingly affects the value of idling losses. Therefore, based on the experience, it is recommended to invest steel with the best characteristics in central and pre-central packages, and in a symmetrical pack you invest steel of the same marks and thicknesses.

6.Compliance with the requirements for transporting and storing open logs and plates.

7. Strict compliance with all tolerances for production deviations. When the parameters of idling are deteriorating, they also depend on the production of any deviations in the assembly, transportation and storage of plates. Use may in transformers cold-rolled steel is very sensitive to mechanical effects. When cutting and punching plates, its magnet properties deteriorate. Strikes on steel, inflections of plates, stickers easily violate the orientation of crystals, increase specific losses and magnetizing power.

8. Introduction to the production of the restorative ignition of the prepared blazes. The burning of plates reduces idling losses by 10-15% by over-distribution and reduction of concentrations of stresses in metal, which are fore sq ft after mechanical processing of plates.

9.Caution of the collector with plates.

In addition to losses in steel, the reduction of the transformer is also caused by losses in the windings of the transformer and additional losses. The reduction of the turn in the windings of transformers from the pressures can be achieved by increasing the section of winding wires. However, this is economically unprofitable, but, as it inevitably increases the size of not only the winding, but also the magnetic wire, that is, increases the mass of active materials and increases the loss of idling, that is, losses in steel transformer.

As for the additional losses in the transformer, they not only reduce the transformer, reducing its efficiency, but also often concentrate in the individual elements of the transformer design, resulting in their dangerous overheating.

Additional losses in parts of the transformer, the causes of their occurrence and ways of elimination are one of the most important tasks, without the permission of which it is impossible to correctly calculate and design the transformer. Equally important are the additional losses for the operation of transformers, as the occurrence of additional losses is often associated with local heating, which under adverse conditions can lead to the premature decommissioning of the transformer [5].

Conclusion

Based on an analysis of the studies carried out to reduce the additional losses, the following is recommended:

1. The most effective way to reduce additional losses is to reduce scattering fields, but they "protect" the transformer from short-circuit currents. The following ways to reduce additional losses are suggested in the given scattering field:

- the direction of scattering flows along paths with fewer losses;
- choosing the right size and configuration of individual elements of the design;
- the use of non-magnetic and non-conductive electrical current materials.

2. Scattering field streams are highly sensitive to magnetic symmetry. A slight displacement of windings relative to each other is enough to dramatically increase the scattering. Such shifts are especially often me hundred in height. For example, one of the windings may not be planted to the end or not how much different in height from the other, which disrupts magnetic symmetry and increases scattering.

Therefore, when planting windings, you need to control their height, not to let the offset of windings. It is also necessary to control the uniformity of the ka naul between the windings and their strictly concentric location on the rod not a magnetic wire.

Magnetic losses can be reduced by the use of magnetic shunts of electrical steel, which can be laid on the shelves of bright beams or along the walls of the tank so that they pass through most of the scattering flow. The vortex currents that occur in them by their magnetic action "push" the scattering field, shielding the tank from it, and thus reduce losses.

3. Significant reductions in additional losses can be achieved through the use of new non-traditional materials for parts of the transformator, such as plastics, fiberglass, layered erasers, etc.

4. The next way to reduce losses is to select small wires, especially in the direction of the perpendicular radial component of the scattering field (to reduce losses from vortex currents); performing transpositions - special transpositions of parallel wires in the process of making windings (to reduce losses from circular currents), reducing the difference of the ditch of bright beams, the use of separate pressing rings for each of the windings (to reduce losses in the elements of the structure).

References

1.Bistriskiy G.F. Choosing and operating power transformers. – M.: Mashinostroenie**,** 2003. – 176 p.

2. Tikhomirov P.M. Power transformers. – M.: Book on Demand, 2012. – 544 p.

3. Farbman S.A. Repair and modernization of transformers. – M.: Book on Demand, 2012. – 554 p.

4. The guide to electric networks 0.4 - 35 kV and 110 - 1150 kV. Power transformers. – M.: Alvis, 2015. – Vol.16. – Book 2. – 704 p.

5. Starodubsev Y.N. Theory and calculation of low-power transformers. – M.: IP RadioSoft, 2015. – 320 p.

Xülasə

Vəliyeva T.D.

Texnoloji emalın elektrotexniki poladın maqnit xüsusiyyətlərinə və transformatorun itkilərinə təsiri

Zərbələrə məruz qalan soyuq yayılan transformator poladı üzərində aparılan tədqiqatlar onun maqnit xüsusiyyətlərinin pisləşməsini göstərir. Poladın keyfiyyətinin pisləşməsi öz növbəsində transformatorda itkilərin artmasına səbəb olur. Işdə transformatorun itkilərinin azadılması üsulu göstərilir ki, bu da transformatorların istehsalında nəzərə alına bilər.

Açar sözlər: polad, itkilər, transformator, itkilərin artması əmsalı, faydalı iş əmsalı, maqnit sahə, maqnit sahəsinin induksiyası.

News of Azerbaijan Higher Technical
Educational Institutions
ISSN 1609-1620
Volume 23, № 5 (2021), 51-59
UDC 621.313.1.2

Research of dynamic processes of the hybrid system

Energetics and energetic machine-building

Khanahmedova S.A.
Azerbaijan State Oil and Industry University
E-mail: samira1009@mail.ru

The dynamic processes of a hybrid system and the main reasons for their creation have been analyzed. Methods for eliminating vibrations during engine start-up are investigated. The kinematics of the elastic unit "hybrid system-crankshaft" is being developed. The equations of motion of a dynamical system are calculated using the Dalamber principle. The calculation is performed for four mass systems. But, according to the obtained data, it is determined that to simplify the comparative analysis and reset the resonances, it is advisable to use the method of electromechanical analogue. Method of electromechanical analogue provides general movement with angular coordinates of all elements of the new complex. The method of electromechanical analogue is used to obtain differential systems of equations that do not take into account the parameters of belt transmission systems.

Keywords: internal combustion engine, engine of a direct current, pulley, inertia, elasticity, shaft, start-switching device.

Introduction

As you know, along with the development of modern industries, serious changes are constantly taking place in all elements of free-moving objects.

In autonomous mobile objects, the start and control of internal combustion engines (ICE) is carried out by systems that contain relatively powerful elements: starter, i.e. a DC machine that performs the start-up process, and a generator provided for power supply.

Based on the generalized theory of electric machines, each electric machine can operate alternately in two modes, that is, the electric machine is two-functional. Following this theory of combining two electric cars, i.e. the use of a hybrid consisting of a starter and generator in cars, is the reason for creating free space in the engine compartment and reducing the consumption of expensive materials. On the other hand, the impact on the environment, reliability, technology, technical and economic indicators and other factors, this task occupies an important place in mechanical engineering.

Changing the mode of operation of a hybrid (single-car) complex, including starting the ICE, switching to generator mode, a sharp change in the speed of the crankshaft in one direction or another, etc. leads to the appearance of dynamic processes.

Statement of the problem

The study of the dynamics of a hybrid mechanism with a conditionally accepted law of change in the current moment, which does not take into account transients in the DC motor and individual nodes, can lead to significant errors. The view of a machine or complex nodes as a system of solid bodies forming kinematic chains is considered outdated. In real mechanisms, almost any link has a

certain degree of malleability. It is known that in any elastic mechanical system with one or more degrees of freedom, free and forced vibrations take place in unsteady processes.

In this single-machine system, vibrations can occur when the moment changes in the motor mode. The reason for these fluctuations may be the start of the DC motor. At the same time, relatively small changes in one of the operating moments can cause alternating stresses in the shafts of the gearbox and the hybrid system. These stresses can lead to the destruction or rapid wear of one or another part of the complex.

Elastic vibrations in the mechanical system of a hybrid complex affect the transients in a DC motor, affecting its speed and torque naturally, there is a relationship between the transients in the mechanical system and the DC machine. This effect is more significant because the complex has elastic elements with relatively low stiffness [1, 2].

This complex refers to mechanisms with a sequential connection of elastic links, working in conditions of free movement of all elements. Fig.1 shows the design diagram of the overall layout of the new hybrid system with ICE.

When starting the ICE, the shafts and belt drive are deformed. The elements included in this construction are connected by elastic links. The movement of these elements is described by a complex system of differential equations, the solution of which is difficult even with the help of mathematical machines. For this reason, of the many elements and relationships between them identify the main, defining the basic character of the movement, and for convenience use the systems given to one of the elements, in this case, the DC motor, i.e. a hybrid system.

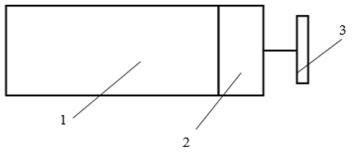

Fig.1. Design of the hybrid system:
1 – DC motor; 2 – starting switch device; 3 – pulley

Solution methods

Analysis of mathematical relations in the calculation of dynamic processes. Let's consider the main mathematical relations used in calculations of reduction of static moments, forces and moments of inertia.

The moment of all elements of the mechanism is driven to the shaft of the hybrid system; the motor shaft is connected to the working body – the crankshaft of the ICE – gear and belt gears [1].

The given static moment is determined by the formula:

$$M_{\mathrm{S}} = M_{\mathrm{m}} \frac{1}{K}, \tag{1}$$

where K – is the gear ratio of the engine to the mechanism, equal to the product of the gear ratios of the gear and belt gears; M_{m} – is the total moment of the elements connected in series.

Moments of inertia are reduced to the same axis, based on the equality of the kinetic energy of the hybrid system and the reduced intermediates. Moments of inertia applied to the DC motor shaft:

$$J_i = J_{\mathrm{m}} + J_1 \frac{\omega_1^2}{\omega_{\mathrm{d}}^2} + J_2 \frac{\omega_2^2}{\omega_{\mathrm{d}}^2}, \tag{2}$$

where J_{i} – moment of inertia applied to the motor shaft; J_{m} – moment of inertia of the rotating parts of the engine; J_1, J_2 – moments of inertia of the shafts of the starting switch and the crankshaft; ω_{d}, ω_1, ω_2 – rotation speeds of the corresponding system nodes.

Taking into account the gear ratios, we get:

$$J_{\mathrm{i}} = J_{\mathrm{d}} + J_1 \frac{1}{k_{\mathrm{d}}^2} + J_2 \frac{1}{k_{\mathrm{d}}^2}. \tag{3}$$

Before proceeding to the reduction operation, you need to determine the stiffness of the links through the stiffness coefficients. As is known, rigidity is the resistance of parts of this mechanism to

deformations under the action of external forces and moments [6]. The proportionality coefficient that exists between the moment and the strain determines the stiffness of the part. To determine the stiffness of various parts, there are expressions depending on their geometric shape and cross-section. In a hybrid system in the ICE start mode, the shafts involved in the moment transmission have an almost constant cross-section. For such a shaft, the torsional stiffness coefficient can be expressed in terms of the modulus and geometric dimensions of the deformable bond. It is defined by the following expression:

$$C_{\text{в}} = \frac{G\pi d^4}{32L}, \tag{4}$$

where G – shear modulus of elasticity; d – the cross-sectional diameter; L – length of the deformable section.

In this structure, the influence of the belt transmission can be introduced in the form of stiffness with the preload:

$$C_{\text{р}} = \frac{2ESr^4}{L}, \tag{5}$$

where E – tensile modulus of steel shaft; S – cross-sectional area of shaft steel; r – the radius of the driving pulley; L – length of the shaft part from the point of action of the moment.

The total stiffness coefficient for this mechanism node will be:

$$C_2 = C_{\text{k}} + C_{\text{p}}. \tag{6}$$

The calculation of the crankshaft stiffness with a belt drive C_3 is also defined as C_2. For this node, the definition of C_{B} and C_{p} stiffness is given using expressions (4) and (5).

The condition of equality of potential energies of the reduced and reduced system is the basis for reducing the stiffness. Since the elastic links of the starter-generator complex are connected in series, we get:

$$\frac{1}{C_{\text{x}}} = \frac{1}{C_1} + \frac{1}{C_2} + \frac{1}{C_3}, \tag{7}$$

where C_{x} – equivalent reduced coefficient of three consecutive elastic links; C_1 – the stiffness coefficient of the shaft of a DC motor; C_2 – stiffness coefficient of the starting switch device; C_3 – coefficient of rigidity of the output part of the crankshaft.

Accordingly, the equivalent malleability coefficient:

$$e_{\text{p}} = e_1 + e_2 + e_3 \tag{8}$$

To draw up an equivalent design scheme of the “hybrid system – crankshaft " mechanism (with elastic mechanical connections) of the link stiffness, we drive it to the DC motor shaft. The kinematic scheme of the mechanism is based on the connected elastic elements: the engine shaft 1, the starting switch device 2, the belt drive 3, and the crankshaft of the internal combustion engine 4 (Fig.2).

Taking into account the gear ratios, we determine the stiffness of individual sections:

$$C_2' = C_2 \frac{1}{K_1^2}; \quad C_3' = C_3 \frac{1}{(K_1 K_2)^2}. \tag{9}$$

The linear calculation system with the general movement of all elements is based on the given kinematic scheme, taking into account the angular coordinates (Fig.2). The angular rotation is taken into account through the gear ratio. For example, if the mass J_3 is rotated by an angle α_2 under the action of the moment M_3, then by drawing the angle of rotation to the motor shaft, we get:

$$\alpha_2' = \alpha_2 K, \tag{10}$$

where K –transmission ratio.

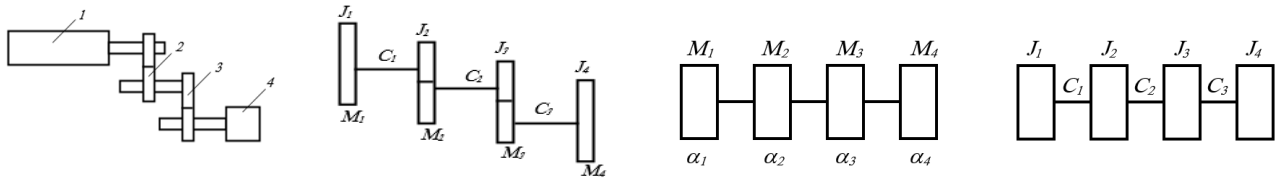

Fig.2. Reduction of the kinematic scheme "hybrid system-crankshaft" with elastic connections:
a – kinematic scheme; *b* – four-mass equivalent scheme;
c – in-line kinematic scheme; *d* – in-line calculation scheme

Equation of motion for the "starter-generator-crankshaft" node and determination of the type of elasticity systems. To create an equation of motion, the rotating system in Fig. 2 can be described by generalized angular coordinates. In the theory of vibrations [6], it is customary to place moving systems by the number of degrees of freedom. Thus, the “hybrid system – crankshaft" calculation system is defined by four generalized coordinates $(\alpha_1,\alpha_2,\alpha_3,\alpha_4)$ and therefore, has four degrees of freedom.

The derivation of the equation of motion can be performed using the Dalambers principle. According to this principle, the dynamics of the system is represented as a static problem; moments and forces due to the inertia of moving concentrated masses are added to the moments or forces acting in the calculation system. Therefore, to create an equation of motion, the record is made in static. According to the Dalambers principle, the dynamic equilibrium condition can be made taking into account the elements of the calculation system connected by elastic bonds:

$$M_{e_{n-1}} - J_n \frac{d_2\alpha_n}{dt^2} + M_n - M_{e_n} = 0\,, \tag{11}$$

where $\frac{d\alpha}{dt} = \omega$ – angular speed of rotation; $M_{e_{n-1}}$ – the moment acting on the *n*-th inertial link, transmitted through the *n*-1 elastic bond, from the element on the left; M_{e_n} – the moment of resistance forces from the side of the *n*+1 inertial link, transmitted through the *n*-th elastic bond, from the element on the right; J_n – moment of inertia of the n-th link; α_n – generalized angular coordinate.

On the other hand, the moment of elastic forces can be expressed in terms of stiffness *C* and angular coordinates α, since the deformation in a non-inertial link, taking into account the transfer to the static system, is linear and obeys Hooke's law:

$$M_{en-1} = C_{n-1}(\alpha_{n-1} - \alpha_n)\,; \tag{12}$$

$$M_{en} = C_n(\alpha_n - \alpha_{n+1})\,. \tag{13}$$

Taking into account (12) and (13), expression (11) can be written as follows:

$$J_n \frac{d\alpha_n}{dt^2} = M_n - C_{n-1}(\alpha_{n-1} - \alpha_n) - C_{n-1}(\alpha_n - \alpha_{n+1})\,. \tag{14}$$

Taking the differentiation symbol $p = d/dt$ for the calculated hybrid system taking into account the crankshaft, we can write the system of the equilibrium equation:

$$\left.\begin{array}{l} J_1 p^2\alpha_1 = M_1 - C_1(\alpha_1 - \alpha_2) \\ J_2 p^2\alpha_2 = M_2 + C_1(\alpha_1 - \alpha_2) - C_2(\alpha_2 - \alpha_3) \\ J_3 p^2\alpha_3 = M_3 + C_2(\alpha_1 - \alpha_3) - C_3(\alpha_3 - \alpha_4) \\ J_4 p^2\alpha_4 = M_4 + C_3(\alpha_3 - \alpha_4) \end{array}\right\} \tag{15}$$

Let's write a differential equation with respect to the angular coordinate α_1(we exclude variables α_2, α_2 and α_4):

$$\frac{J_1J_2J_3J_4}{C_1C_2C_3}p^8\alpha_1+\left(\frac{J_1J_2J_3}{C_1C_2}+\frac{J_1J_2J_4}{C_1C_3}+\frac{J_1J_2J_4}{C_1C_2}+\frac{J_1J_3J_4}{C_1C_3}+\frac{J_1J_3J_4}{C_2C_3}+\frac{J_1J_3J_4}{C_2C_3}\right)p^6\alpha_1+$$
$$+\left(\frac{J_2J_3}{C_1}+\frac{J_1J_2}{C_1}+\frac{J_1J_3}{C_2}+\frac{J_1J_4}{C_1}+\frac{J_2J_3}{C_2}+\frac{J_3J_4}{C_2}+\frac{J_1J_4}{C_2}+\frac{J_1J_4}{C_3}++\frac{J_3J_4}{C_3}\right)p^4\alpha_1+(J_1+J_2+J_3+J_4)p^2\alpha_1=$$
$$=M_1+M_2+M_3+M_4+\frac{J_2J_3J_4}{C_1C_2C_3}p^6M_1+\left(\frac{J_2J_3}{C_1C_2}+\frac{J_3J_4}{C_2C_3}+\frac{J_3J_4}{C_1C_2}+\frac{J_2J_4}{C_1C_3}+\frac{J_2J_4}{C_1C_2}\right)p^4M_1+$$
$$+\left(\frac{J_2}{C_1}+\frac{J_3}{C_1}+\frac{J_4}{C_2}+\frac{J_4}{C_1}+\frac{J_4}{C_2}+\frac{J_4}{C_3}\right)p^2M_1+\frac{J_3J_4}{C_2C_3}p^4M_2+\left(\frac{J_3}{C_2}+\frac{J_4}{C_3}+\frac{J_4}{C_2}\right)p^2M_2+\frac{J_4}{C_3}p^2M_3 \quad (16)$$

In general, the equation of motion of in-line calculation systems of an electric drive, taking into account elastic mechanical connections, is written in the following form [5]:

$$\sum_{i=1}^{n}\left(A_i p^{2i}\alpha_1\right)+\alpha_1=\sum_{i=1}^{n}\left(B_i M_i\right)+f\left(M_1,...,M_{n-1}\right), \quad (17)$$

where n – number of degrees of freedom.

The left part of equation (17) is the sum of even derivatives of the desired coordinate with coefficients A_i depending on the moments of inertia and stiffness of elastic links and the coordinate α_1. The right part consists of two parts: the first part is the sum of all the moments acting in the system with coefficients that also depend on the moments of inertia and stiffness. The second part is a function of the sum of even derivatives of acting moments with coefficients

Taking into account the generalized equation (17) for the hybrid system-crankshaft, we write equation (16) in the following form:

$$A_4p^8\alpha_1+A_3p^6\alpha_1+A_2p^4\alpha_1+A_1p^2\alpha_1=B_3p^6M_1+B_2p^4M_1+B_1p^2M_1+$$
$$+C_2p^4M_2+C_1p^2M_2+Dp^2M_3+M_1+M_2+M_3+M_4, \quad (18)$$

where *A*, *B*, *C* and *D* can be determined by equation (17) written for this system.

The considered examples [4, 5] explain the processes of transition from the kinematic scheme of an electric drive to its reduced design mechanical scheme and the possibility of simplifying the latter. It is noted that completely different types of mechanisms are reduced to three-mass or two-mass elastic systems. Taking into account this distribution of typical design schemes, the design scheme of the mechanism refers to a four-mass elastic system, which is used in the study of electromechanical systems of an automated electric drive in rare cases when there is a need for a more detailed analysis of the movement conditions of their mechanical part. In such cases, mathematical modeling on computers is usually used to solve the problem. To study individual physical features of four-and three-mass systems, it is usually reduced to a two-mass elastic system with two degrees of freedom, which is the main object of research in the theory of automated electric drive [3].

For an electric drive system, “hybrid complex-crankshaft " is an object that has in its design a belt transmission between the shaft of the starting switch device (gearbox) and the crankshaft. The processes occurring in the crankshaft are almost not transferred to the gearbox shaft except for the moment of resistance due to the increased elasticity of the belt.

These processes associated with compression of the mixture in the ICE cylinder, are not constant in frequency of occurrence in the system "crankshaft-belt transmission". Accounting for all these high-frequency forces in the mathematical system of research, varying in amplitude, time, frequency, and shape, is very difficult, and with a short - term starter generator, accounting for these phenomena will not bring much benefit in any positive output approach [4].

In addition, all high-frequency moments acting on the crankshaft are extinguished by the flywheel rigidly connected to the crankshaft, and the elasticity of the belt drive. Given this fact, it can be concluded on the transfer system in two-mass (Fig.3).

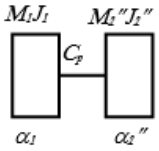

Fig. 3. Two-mass elastic system of the mechanism
"hybrid system-crankshaft".

Included in this design scheme, the moments of rigidity and moments of inertia of links are given with the coefficients of transmission and angular displacement expressions (1), (3), (7), (10). In this case, the equilibrium equations of a system with two degrees of freedom will be:

$$\left.\begin{aligned} J_1 p^2 \alpha_1 &= M_1 + C_{p1}\left(\alpha_1 - \alpha_2''\right) \\ J_2'' p^2 \alpha_2'' &= M_2'' + C_p\left(\alpha_1 - \alpha_2''\right) \end{aligned}\right\}, \tag{19}$$

where J_2'', M'', C_p – accordingly, the values of the moment of inertia, the moment of resistance and the stiffness of the elements shown on the shaft of the hybrid system. They are also easily determined by equations (1), (3) and (7).

The joint solution of system (19) with respect to α_1 gives the equations of this two-mass system:

$$\frac{J_1 J_2''}{C_p} p^4 \alpha_1 + \left(J_1 + J_2''\right) p^2 \alpha_1 = M_1 + M_2'' + \frac{J_2''}{C_p} p^2 M_1 . \tag{20}$$

For this case, it is easy to find the sum of partial derivatives of the desired coordinate with coefficients Ai acting in the system of moments with inertia and stiffness coefficients included in the general drive equation “hybrid system – crankshaft” (19).

in the resulting differential equations, all the mechanical parameters of all four nodes are implicitly involved, which makes them difficult to compare. in order to justify this assumption, the method of electromechanical analogue is used to derive the equation of moments acting on the same shaft of the starter-generator complex (Fig. 4). This method is widely used in the theories of electromechanical vibrations and electrical devices [5].

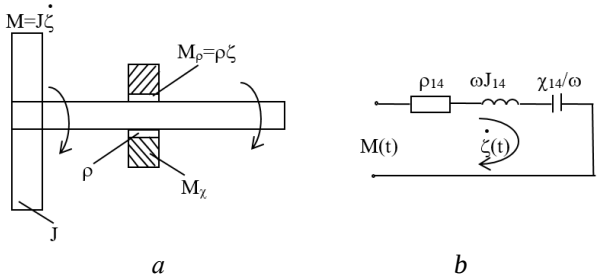

Fig. 4. Equivalent circuit of a single-mass mechanical device (*a*) and
replacement circuit of a mechanical circuit (*b*)

To begin with, the vector value of the periodic forces acting on the body of the mechanism is determined:

$$F = F_0\left(\cos\,\omega t + j \sin\,\omega t\right) = F_0 e^{j\omega t} . \tag{21}$$

Similarly, for linear motion, we write the following expression:

$$V = V_0\left(\cos\,\omega t + j \sin\,\omega t\right) = V_0 e^{j\omega t} \tag{22}$$

If you keep in mind that the speed value is expressed as follow:

$$\dot{V} = j\omega\left(V_0 e^{j\omega t}\right) = j\omega t \quad \text{and} \quad V = \frac{\dot{V}}{j\omega}, \tag{23}$$

and then we get:

$$\dot{V} = j\omega\left(j\omega V_0 e^{j\omega t}\right) = j\omega\dot{V}\left(j\omega\right)^2 V = -\omega^2 V \tag{24}$$

$$\dot{V} = j\omega\dot{V}$$

According to the Dalambers principle amount determined by the following values:

1. the total value of the speeds acting on individual nodes:

$$\dot{V} - \dot{V}_m - \dot{V}_r - \dot{V}_k = 0; \tag{25}$$

2. Total value of forces acting on individual nodes:

$$F - F_m - F_r - F_k = 0\ , \tag{26}$$

where *m*, *r* and *k* – indices are parameters that provide for inertia, friction, and elasticity.

We will write the speed expression in the following form:

$$\dot{V}_m = \frac{F_m}{m} \text{ or } \dot{V}_m = \frac{1}{m}\int F_m dt = \frac{F_m}{pm}, \tag{27}$$

$$\dot{V}_r = \frac{F_r}{r}; \tag{28}$$

$$V_k = \frac{F_k}{k} \text{ or } \dot{V}_k = \frac{1}{k}\frac{dF_k}{dt} = \frac{pF_k}{k} \tag{29}$$

Let's write these expressions in (25):

$$\dot{V} - \frac{F_m}{pm} - \frac{F_r}{r} - \frac{pF_k}{k} = 0, \tag{30}$$

and the values of the forces F_m, F_r and F_k will have the following form:

$$F_m = m\dot{V} = j\omega\dot{V};\ F_r = r\dot{V}; F_k = kV = \frac{k}{j\omega}\dot{V} \tag{31}$$

Force acting on the shaft:

$$F = \left(r + \frac{k}{j\omega} + j\omega m\right)\dot{V} = r + j\left(\omega m - \frac{k}{\omega}\right)\dot{V} = z\ , \tag{32}$$

where *z* – mechanical resistance in linear motion,

$$z = \frac{F}{V} = r + j\left(\omega m - \frac{k}{\omega}\right) \tag{33}$$

Similarly, according to the scheme shown in Fig. 4, a we write the following expressions:

$$\mathrm{M_j} = \mathrm{J}\dot{\zeta} = \mathrm{j}\omega\mathrm{J}\dot{\zeta};\ \mathrm{M_\rho} = \rho\dot{\zeta}; \tag{34}$$

$$\mathrm{M_\chi} = \chi\zeta = \frac{\chi}{\mathrm{j}\omega}\dot{\zeta}; \tag{35}$$

$$\mathrm{z} = \frac{\mathrm{M}}{\dot{\zeta}} = \rho + \mathrm{j}\omega\mathrm{J} + \frac{\chi}{\mathrm{j}\omega} = \rho + \mathrm{j}\omega\left(\mathrm{J} - \frac{\chi}{\omega^2}\right). \tag{36}$$

where $\dot{\zeta}$ – angular speed of rotation; χ – the elasticity of the node.

The equivalent circuit of the mechanical circuit (Fig.4*б*)

$$\dot{\zeta} = \frac{M(t)}{\chi + j\omega J + \frac{\chi}{j\omega}} = \frac{M(t)}{\rho + j\omega\left(J - \frac{\chi}{\omega^2}\right)}. \tag{37}$$

For a four-mass system:

$$\dot{\zeta}(t)=\frac{M(t)}{z_1+z_2+z_3+z_4}= \\ =\frac{M(t)}{\rho_1+\rho_2+\rho_3+\rho_4+j\omega\left(J_1+J_2+J_3+J_4-\frac{\chi_1+\chi_2+\chi_3+\chi_4}{\omega^2}\right)}. \quad (38)$$

Due to the insignificance of the friction force and the mass of the belt drive, we neglect the parameters ρ_2, ρ_3, J_2 and J_3, and for the angular velocity of rotation through the moment of rotation M(t) and the mechanical resistance z_m, we obtain the following analytical expression:

$$\dot{\zeta}=\frac{M(t)}{\rho_1+\rho_4+j\omega\left(J_1+J_4-\frac{\chi_1+\chi_4}{\omega^2}\right)}, \quad (39)$$

From the conditions $J_1+J_4=\frac{\chi_1+\chi_4}{\omega^2}$ we obtain an analytical expression for the resonant part:

$$\omega_0=\frac{1}{\sqrt{\left(J_1+J_2\right)\left(\frac{1}{\chi_1+\chi_2}\right)}}. \quad (40)$$

The denominator of the expression (40) is quite large, so the resonance is possible at low frequencies $\omega = \omega_0$.

The hybrid design makes it possible to bring a four-mass node into a two-mass system.

Conclusion

1. Dynamic processes, causes of friction and vibration are investigated, and problems for their elimination are solved.

2. Developed kinematics elastic knot "hybrid system-crankshaft", the settlement system of a number based on the kinematic scheme providing for common movement with the angular coordinates of all elements of the complex.

3. Due to the implicit participation in the obtained differential equations of the mechanical parameters of all four nodes, for their comparative analysis, the method of electromechanical analogue is used and differential systems of equations are obtained that do not take into account the parameters of belt transmission systems.

4. It was found that the design of the hybrid complex makes it possible to bring the four-mass "hybrid system-crankshaft" node into two-mass elastic system.

References

1. Farkhadzade E.M., Aliyev E.S., Khanahmedova S.A. Electric drive part I. // Textbook, Azerbaijan State Oil Academy Publishing House. – Baku, 2010.

2. Erokhin M.N. Machine parts and design basics. // http://booktech.ru/books/detali-mashin/139-detali-mashin-i-osnovy-konstruirovaniya-2005-pod-red-mn-erohina.html. – 2005.

3. Nysret Avdiu, Shaban Buza. Analysis of the multi-mass drive system dynamics with induction motor // https://www.tmt.unze.ba/zbornik/TMT2011/076-TMT11-142.pdf. – 2011.

4. Timothy M. O'Sullivan, Bingham C., Schofield N. Observer-Based Tuning of Two-inertia servo-drive systems with integrated saw torque transducers // https://www.semanticscholar. org/paper/Observer-Based-Tuning-of-Two-Inertia-Servo-Drive-O'Sullivan-Bingham, 2007.

5. Szabat K., Orlowska-Kowalska T. Analysis of the multi-mass drive system dynamics using reduced-order mathematical model. // https://www.semanticscholar.org/paper/Analysis-of-the-multi-mass-drive-system-dynamics-Szabat-Orlowska-Kowalska. – 2013.

Xülasə
Xanəhmədova S.Ə.
Hibrid sistemin dinamik proseslərinin tədqiqi

Hibrid sistemin dinamik prosesləri və onların meydana gəlməsinin əsas səbəbləri təhlil edilir. Mühərrikin işə salınması zamanı vibrasiyaların aradan qaldırılması üsulları tədqiq edilmişdir. Yeni kompleksin bütün elementlərinin bucaq koordinatları ilə ümumi hərəkətini təmin edən "hibrid sistem-dirsəkli val" elastik qovşağının kinematikası işlənilir**.** Dalamber prinsipinə əsaslanaraq dinamik proseslərin hərəkət tənlikləri hesablanır. Hesablama dördkütləli sistem üçün yerinə yetirilir. Lakin alınan nətıcələrə əsasən müəyyən edilir ki, müqayisəli təhlilin sadələşdirilməsi və rezonansların sıfıra yaxınlaşması üçün elektromexaniki analogiya metodundan istifadə edilməsi məqsədəuyğundur. Elektromexaniki analogiya metodu ilə ötürücü qayış sistemlərinin parametrlərini nəzərə almayan diferensial tənliklərin sistemlərinin əldə edilməsi üçün istifadə olunur. Məqalədə ikikütləli elastik sistemə keçməyə imkan verən dördkütləli hibrid sistemin konstruksiyası nəzərdən keçirilmişdir.

Açar sözlər: daxili yanma mühərriki, sabit cərəyan mühərriki, şkiv, ətalət, elastiklik, val, işəsalıcı-çevirici qurğu.

Ünvan: AZ1010, Bakı, Azadlıq prospekti, 20
Telefon: (99412) 598-44-77; Faks: (99412) 598-65-61
Elektron poçtu: AATMX@asoiu.edu.az

Jurnal 1999-cu ilin iyun ayından nəşr olunur